

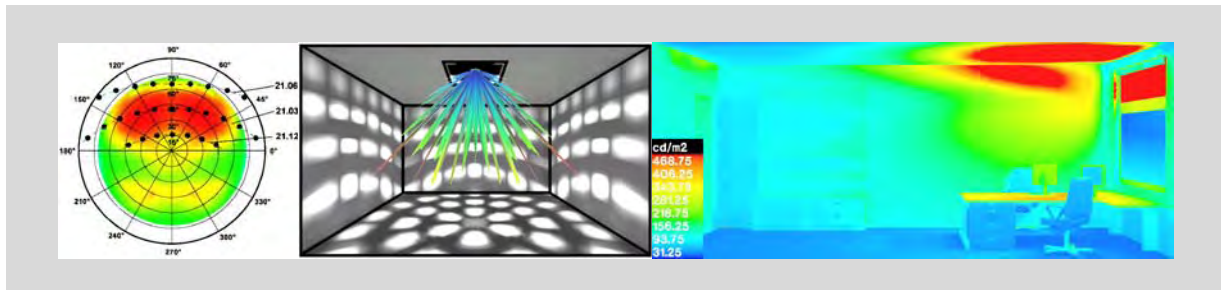
DRAFT

Modelling Indoor Illumination by Complex Fenestration Systems Based on Bidirectional Photometric Data

A Report

of IEA SHC TASK 31 DAYLIGHTING BUILDINGS IN THE 21ST CENTURY

April 2005



This report was prepared as an account of work sponsored by the Government of the Federal Republic of Germany and the ADELINe Users Club.

Neither the Federal Republic of Germany, nor the ADELINe Users Club, nor the International Energy Agency, nor any of their employees, nor any of their contractors, subcontractors, or their employees makes any warranty, express or implied, or assumes legal liability or responsibility for the accuracy, completeness or usefulness of any information, apparatus, product or product disclosed, or represents that its use would not infringe privately owned rights.

This report was printed and is available at:

Fraunhofer-Institut für Bauphysik
Nobelstr. 12
70569 Stuttgart, Germany
Fax: +49-711-970-3399
Price: 15,- €

Modelling Indoor Illumination by Complex Fenestration Systems Based on Bidirectional Photometric Data

**International Energy Agency (IEA)
Solar Heating and Cooling Programme Task 31**

**DAYLIGHTING BUILDINGS IN THE 21ST
CENTURY**

DISTRIBUTION CLASSIFICATION: UNRESTRICTED

PREFACE

The main objective of IEA Solar Heating and Cooling Programme (SHC) Task 31 “Daylighting Buildings in the 21st century” is to make daylighting the typical and preferred design solution for lighting buildings in the 21st century by integrating human response with the application of daylighting systems and shading and electric light control strategies. Two key issues, which require research to accomplish energy savings, have been identified as:

- The determination of occupant response towards the luminous and thermal environments in buildings using daylighting systems and daylight responsive controls.
- The integration of daylighting systems, electric lighting, and shading controls taking into account occupant response in order to optimise energy savings.

A third objective is to ensure transference of the results to building design professionals, building owners, and manufacturers. The Task will focus on commercial buildings, both new and existing, including office, retail, and institutional buildings such as schools. The participants in this task are Australia, Belgium, Canada, Denmark, Finland, France, Germany, Italy, Japan, Netherlands, New Zealand, Norway, Sweden, Switzerland, United Kingdom and the United States. Australia is the Operating Agent.

The objective of this Subtask C “Daylighting Design Tools” is to improve the knowledge and quality of lighting tools to enable building designers to predict the energy performance and visual comfort conditions of complex fenestration systems in their daily working process. This Subtask will make a link between industry, designers and software developers and promote the tools to the practitioners. Subtask C is comprised of the following projects:

C1: User Interactions

C2: Algorithms and Plug-Ins

C3: Promotion of Tools & Engines

C4: Validation

EXECUTIVE SUMMARY

The document presents work conducted as part of Subtask C, “Daylighting Design Tools”, Subgroup C2 “Algorithms and Plug-Ins“, of the IEA SHC Task 31 “Daylighting Buildings in the 21st century”.

Significant efforts to assess the Bidirectional Transmittance distribution Functions (BTDFs) of complex fenestration systems (CFS) have been undertaken in recent years. This paper presents a methodology for including these bidirectional photometric raw data sets into the daylighting simulation and design process. The method is based on computing the luminous intensity distribution on internal façade elements from BTDF data (measured or calculated) and the outside luminance distribution on the façade elements. Special designed filters, which are necessary to pre-process the raw data, are derived. Since the BTDF raw data sets are big in volume, data compression techniques are introduced and applied. In order to account for dynamic – i.e. time variant systems – façade systems, like automated blinds, control models are being provided. The method is exemplarily incorporated into a complex fenestration system database and lighting simulation engines. The procedure is being validated. Limitations of the method are being discussed.

Contents

Nomenclature	2
1. Introduction	4
2. Review of Complex Fenestration System (CFS) models	5
2.1 Photometry of CFS	5
2.1.1 Quantities	5
2.1.2 Data assessment methods (Goniophotometry)	8
2.2. Modelling CFS in daylight simulation	9
3. CFS model based on bidirectional photometric data	12
3.1 Light transmittance under diffuse illumination	15
3.2 Light transmittance under direct illumination	20
4. Incorporation into daylight simulation	25
4.1 Photometric aspects	25
4.2 Dynamic systems	27
4.3 Application Programming Interface	29
4.3 CFS database	29
4.4 Interfaces to lighting calculation engines	31
5. Accuracy and validation	33
5.1 Accuracy	33
5.2 Validation	38
6. Conclusion	43
7. References	44
8. List of Contact Persons	46
9. IEA Information	47

Nomenclature

a	similarity measure	[-]
A	surface	[m ²]
c	transform coefficient	[-]
E	illuminance	[lx]
f	original function (raw data)	[-]
h	height	[m]
I	luminous intensity	[cd]
L	luminance	[cd/m ²]
\bar{n}	normal vector	[-]
P	point on worksurface	[-]
q	luminance coefficient	[cd/m ² /lx]
r	distance	[m]
S	visibility function	[-]
X	point on surface	[-]

Greek letters

γ	altitude (angle)	[°]
τ	light transmittance	[-]
φ	azimuth angle	[°]
Φ	luminous flux	[lm]
χ	set of all points X on a surface	[-]
ψ	basis function	[-]
$\vec{\omega}$	direction vector	[-]
Ω	solid angle	[sr]
$d\omega$	solid angle element	[sr]

Subscripts

a	emerging side
d	discrete
diff	diffuse
e	incident side

F	façade element
fi	filtered
m	mean
r	reflected (room-side)
S	solar, sun

1. Introduction

Aside from fulfilling acoustical, indoor-climate and energetic functions, façades can nowadays efficiently supply natural lighting to interior spaces. On the one hand, they have to provide an appropriate visual indoor environment; on the other hand, daylight penetrating the room through the façades should favourably influence the overall building energy balance. Daylight utilization can directly reduce energy consumption for electric lighting and can indirectly - due to the higher luminous efficacy of daylight compared to commonly used artificial lighting systems - reduce the thermal loads within the conditioned building spaces. Therefore various new façade components aiming at a better daylight supply – while still providing sufficient solar and glare protection - have been developed. Due to this, serious efforts to assess the photometry of these complex fenestration systems (CFS) have been undertaken in recent years [1][2]. Nevertheless the use of these photometric datasets in support of daily design decisions still appears to be moderate. The reasons are obvious: The raw data sets are of high complexity and do not directly relate to the later room illumination under specific boundary conditions. A lack of appropriate calculation models inhibits the use of these data-sets in daylighting design practice. This paper therefore presents an approach, which seeks to overcome these obstacles.

For determining the impact of different complex fenestration systems on room illumination and lighting energy demand, a calculation method has been developed. It is based on measured or calculated bidirectional data sets describing the façade systems' photometry. The method is independent of specific lighting simulation programmes and generally can be plugged into different standalone tools. Aside from optimising façade components as early as in the development stage, the method allows for detailed quantitative, lighting and energetic evaluations of different façade systems in daylighting design.

Since the bidirectional data sets are being recorded for a restricted number of incident angles [1] - generally the subdivision of the hemisphere according to Tregenza [3] is used - the data resolution on the incident side is normally significantly lower than the resolution on the emerging hemisphere.

Implementing these raw data directly into superposition algorithms results - as will be shown - in artefacts and wrong predictions of the luminous intensity distribution. Therefore, based on the geometric relations of the hemispherical subdivision scheme, a special designed filter, which is necessary to pre-process the raw data, is derived. Since the photometric raw data sets are big in volume, data compression techniques are introduced and applied. One compression technique is closely related to the filtering of the data, which generally allows significant down sampling, the other technique involves a wavelet transform. In order to account for dynamic – i.e. time variant – façade systems (like automated blinds) control models are being provided. The methods are exemplarily incorporated into a complex fenestration system database and lighting simulation engines. The procedure is being validated for selected test cases. Limitations of the method are being discussed.

2. Review of Complex Fenestration System (CFS) models

2.1 Photometry of CFS

2.1.1 Quantities

The coordinate system for the description of façade systems according to the format defined within IEA Task 21 [1] is presented in Figure 1. The transmittance behaviour of clear single-pane and multi-pane glazing systems can be stated by the light transmittance τ according to DIN EN 410 [4]. This value applies to quasi-parallel, perpendicular incidence of light. In [5], methods for determining the angle-dependent light transmittance are compiled. Façade components with more complex transmittance characteristics require a more detailed description of the direction-dependent light transmittance. The transmittance

$$\tau(\bar{\omega}_e) = \frac{\Phi_a}{\Phi_e(\bar{\omega}_e)} \quad [-] \quad (1)$$

describes the ratio of the luminous flux ϕ_a , which has been transmitted through the system, and the incident luminous flux ϕ_e , for a defined direction of light incidence. The coefficient is determined by measurement, using integrating spheres [1]. Exemplary directional hemispherical transmittances for a clear glazing system and for a light redirecting glass [1] are depicted in Figure 2 as a function of the incident direction. The distributions for a vertical,

south-oriented façade are superimposed with the solar positions at winter solstice, at equinox and at summer solstice. Whereas the clear glazing has symmetrical distribution characteristics, the light redirecting glass has a relatively higher transmittance into the upper half of the emerging side hemisphere. The light redirecting glass was specially designed for the transmittance of direct light, which is redirected into the upper half of the emerging side's hemisphere as will be described in the following.

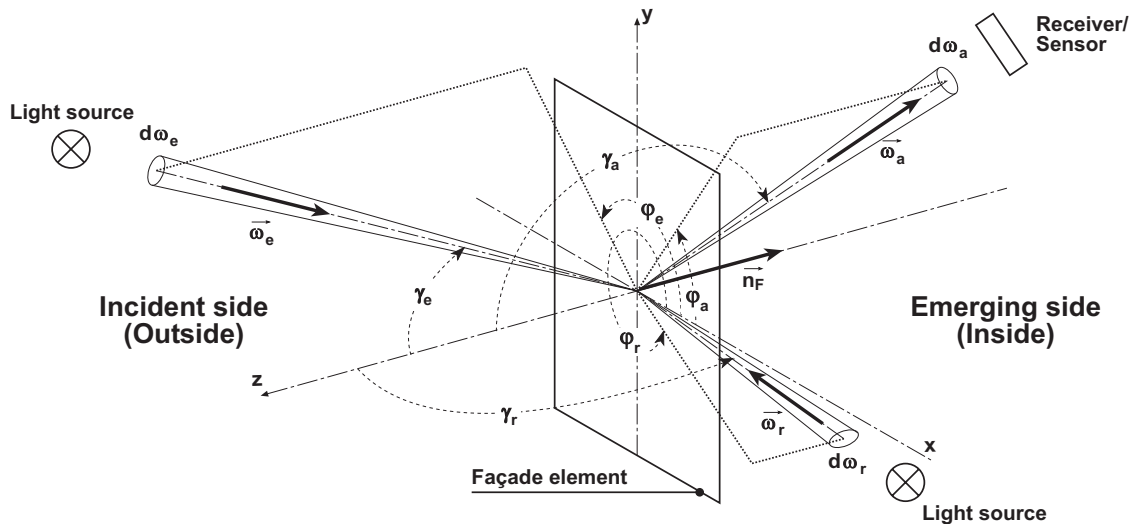


Figure 1: Coordinate system for the description of the directions of light incidence and emerging light on a façade element following [1].

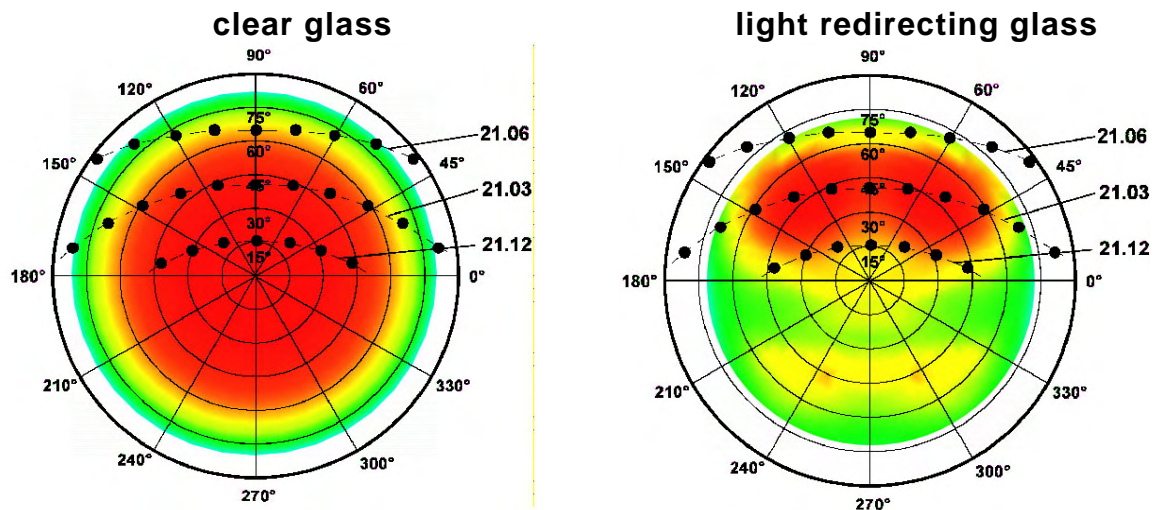


Figure 2: Representation of the directional hemispherical light transmittance through clear glass and through light redirecting glass acc. to [1], given in polar coordinates. System characterisation by superimposition of the ecliptics at winter and summer solstice and equinox for a vertical south-orientated façade.

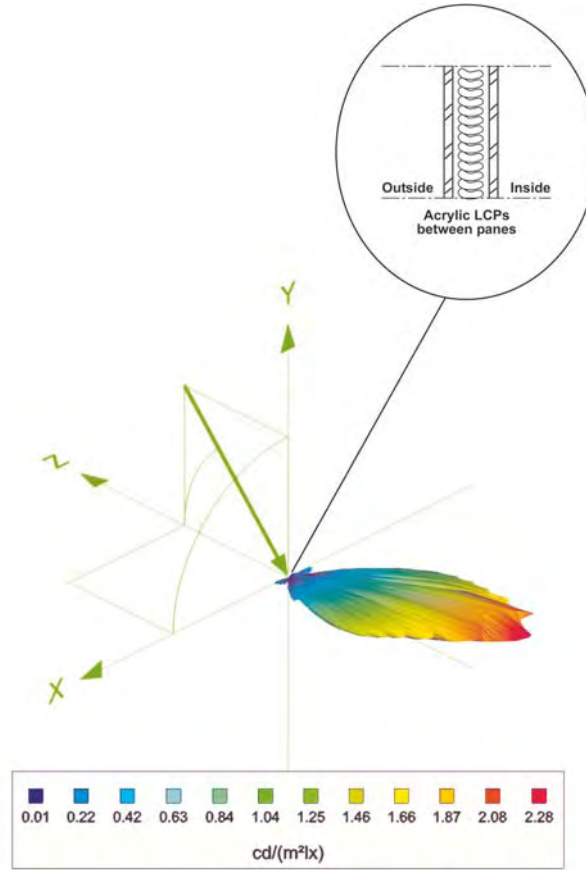


Figure 3: Indicatrix of diffusion for a light redirecting glass acc. to [1] for a light incidence under $\gamma_e = 48^\circ$, $\varphi_e = 90^\circ$. Representation of emerging side luminances in spherical coordinates.

To describe the spatial distribution of the transmitted and also reflected light the luminous coefficient is used:

$$q(\vec{\omega}_e, \vec{\omega}_a) = \frac{L(\vec{\omega}_a)}{E(\vec{\omega}_e)} \left[\frac{\text{cd}}{\text{m}^2 \cdot \text{lx}} \right] \quad (2)$$

with

$$E(\vec{\omega}_e) = L(\vec{\omega}_e) \langle -\vec{n}_F, \vec{\omega}_e \rangle d\omega_e \quad [\text{lx}]. \quad (3)$$

The luminous coefficient describes the luminance L , which is visible under the angles of observation $\vec{\omega}_a$ (see Figure 1), induced by illuminance E , which is generated by a light source with incident direction $\vec{\omega}_e$. The spatial distribution of the luminous coefficient is referred to as indicatrix of diffusion or Bidirectional Transmittance Distribution Function, abbreviated BTDF. By

analogy with the light transmittance behaviour, the indicatrix of diffusion may be formulated for the reflection of light, also referred to as Bidirectional Reflection Distribution Function, abbreviated BRDF. Figure 3 presents an exemplary indicatrix of diffusion for the transmittance of a light redirecting glass acc. to [1], for a given illumination under an altitude of 48° and an azimuth angle of 90° . The redirection of daylight into the upper half of the emerging side's hemisphere can be observed. Moreover, the diffusing effect of the glazing becomes obvious.

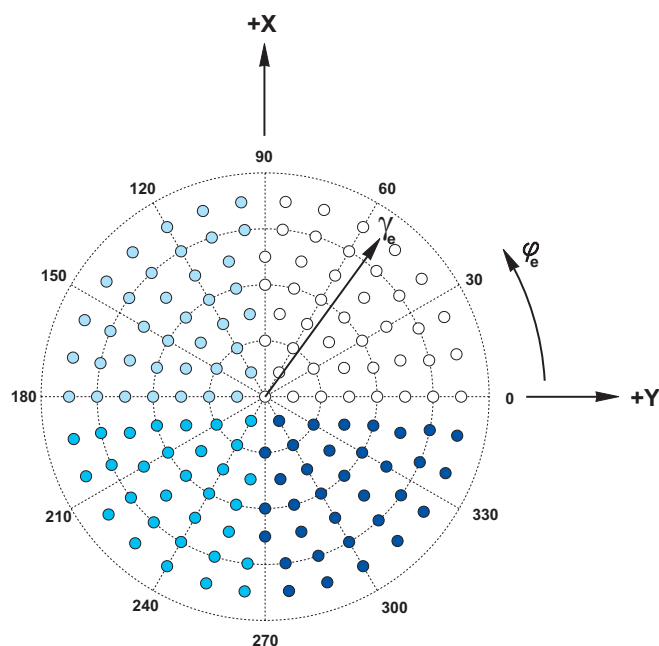


Figure 4: Incident angles according to the Tregenza subdivision scheme [3]. Symmetries of the subdivision scheme are indicated

2.1.2 Data assessment methods (Goniophotometry)

The indicatrices of diffusion may be determined by means of goniophotometry on the basis of a measurement protocol, which was defined in an international collaborative project within the framework of IEA-SHC-ECBCS Task 21 'Daylight in Buildings' [1]. Depending on the symmetrical properties of the sample, indicatrices of diffusion are determined according to Tregenza [3] for up to 145 incident directions, which are approximately uniformly distributed over the incident-side hemisphere (see Figure 4). An elaborated overview on how to obtain measured and calculated datasets is given under [2]. The overview – in addition - holds a list of the divers datasets available nowadays. For incorporation into lighting simulation tools - according to the method described in this paper - complete BTDF datasets are mandatory. Therefore,

indicatrices have to be provided for all 145 incident angles. For dynamic systems, like venetian blinds with different slat inclines, complete datasets for the distinct angular positions are necessary. The principle of the methodology developed in section 3 is general. Within this paper, it is specifically adapted to the above mentioned measurement protocol.

2.2. Modelling CFS in daylight simulation

The general calculation of photometric quantities and the visualization of outdoor and indoor lighting scenarios are nowadays basically relying on either radiosity or backward ray-tracing methods [6]. They have been implemented in numerous variations either separately [7], [8] or also as combined approaches [9]. Both the radiosity method and the backward ray-tracing method are subject to limitations when modelling light transmittance through geometrically and material-wise complex fenestration systems. Implementations of the above mentioned methods are generally capable of considering simple glazing models. Both methods are able to consider components with diffuse transmittance properties and clear glazing, here taking into account the Fresnel equations [10] (i.e. the angular dependency of light transmittance). In addition, diffusely reflecting slatted blinds can be modelled. Radiosity methods are restricted to surfaces with diffuse reflection; hence, they are generally incapable of considering façade components with specular reflecting surfaces. Backward ray-tracing techniques, such as the RADIANCE programme system [8], offer interfaces facilitating external functional definitions of further systems. In this way it is possible to model façade components that are based on the refraction of light (like prismatic elements) [8] and laser-cut panels [11], whose geometry can be parametrized to a limited extent. Using plane mirrors, scenes can be indirectly lit by means of so-called virtual light sources. Due to the algorithmic efficiency, this procedure however remains limited to a few mirrored plane surfaces that are interreflecting light. Modelling-limitations [8] arise for

- façade systems with mirrored surfaces, which are for instance composed of layered, plane, or curved high gloss finished aluminium slats,
- façade systems based on diffraction phenomena, like holographic-optical elements and

- façade components containing local, stochastically varying structures like diffusely scattering inserts or special light redirecting glass [12].

These modelling limitations can be tackled by different approaches. One option is the extension of the existing backward ray-tracing techniques by involving forward ray-tracing techniques. On the other hand, integration of CFS into lighting simulation on the basis of measured or numerically predetermined indicatrices of diffusion can be pursued.

Extension of simulation programmes by forward ray-tracing techniques

Presently, the so-called photon mapping technique [13], a special kind of forward ray-tracing technique, is being implemented into RADIANCE as a supplementary programme module promising to extend the capabilities of the RADIANCE programme system significantly. Another extension of RADIANCE, the commercial 'Raydirect' programme module [14], presents an approach for mapping the light transmittance through façade systems by inclusion of a simple forward ray-tracing technique [15]. The technique is subject to the restriction that only materials with ideal reflection and ideal refraction can be rendered. The system structures that can be modelled remain restricted to two-dimensional extruded profiles. In [17] the integration of a forward ray-tracing technique into another lighting simulation engine, the software Genelux, is reported. As with all ray-tracing techniques, wave optics phenomena cannot be treated. Accordingly, holographic optical elements cannot be modelled by way of this approach. Forward ray-tracing techniques, which still rely on (deterministic) assumptions of the geometric and material properties of CFS, do not per se offer approaches to handle CFS with stochastically varying geometric and material characteristics. These are numerically difficult to model and may often be better described by measurements. Approaches incorporating forward-ray-tracing techniques so far are proprietary solutions, which are linked to specific programme systems and are often complex to apply, i.e. remain restricted to a highly skilled community.

Extension of simulation programmes based on bidirectional photometric data (indicatrices of diffusion)

A solution that is based on a description of the system's behaviour by means of indicatrices of diffusion is generally independent of the type of calculation algorithm and, accordingly, therefore also independent of a specific lighting

calculation programme. The capability of immediately considering measured system performance data may spare modelling system components of partially complex geometries and materials and excludes error sources due to faulty input specifications. Hard-to-model façade components that contain local, stochastically varying structures like diffuse inserts or special light-redirecting glazing, can be considered on a basis of measured data. Holographic optical elements can also be analysed on such a basis. Nevertheless it may be argued, that indicatrices of diffusion are today still difficult to obtain and only a few complete descriptions of CFS exist. Significant efforts among other things within IEA Task 31 [2] have been undertaken to overcome this shortage. Numerous physically measured data sets are available nowadays. New calculation procedures, numerical goniophotometric approaches, have been developed, allowing also the computation based determination of system behaviour [16] according to the measurement protocol described in section 2.1. For a few CFS, system-specific modelling approaches were proprietarily implemented into selected lighting calculation programmes, thus allowing to predict indoor illumination by the systems. For instance, the integration of the light redirecting glass [12] that was measured within the framework of IEA Task 21 [1] in the RADIANCE environment is reported in [18]. However, the adopted approach is only applicable to highly scattering materials with properties comparable to those of the light redirecting glass. The approach is not suited for systems with indicatrices of diffusion with strong spatial resolutions, i.e. high frequency components. If these luminous coefficients are directly superimposed, illumination of the interior spaces by the fenestration system is generally represented highly falsified. The effect will be demonstrated within chapter 3.1 (see Figure 8 and Figure 9). For a qualitative examination of the light transmittance properties, luminous intensity distributions of a specific slat configuration are determined in [19] in an approximate solution. These have been integrated as luminaires into the lighting simulation programme DIALUX [20].

Therefore, at present, the performance of CFS under real sky luminance distributions within a built environment can only be modelled for a few systems under partially strict boundary conditions. A procedure allowing to handle arbitrary measured or as well calculated CFS descriptions based on indicatrices of diffusion can help to overcome this shortage.

3. CFS model based on bidirectional photometric data

In the following, a general calculation method is developed that allows the determination of room illumination by different CFS based on bidirectional photometric data. The approach intends to overcome some of the restrictions addressed in the previous section. A scheme of the calculation method is presented in Figure 5, the individual steps are introduced in Figure 6. Measured or calculated external luminance distributions are processed with the actual photometric data of the CFS, resulting in luminous intensity distributions, which are then used to calculate the indoor lighting environment in the so called direct calculation, i.e. the determination of the primary light contribution to the space by the light sources in the scene only. The method can be embedded into various lighting simulation programmes.

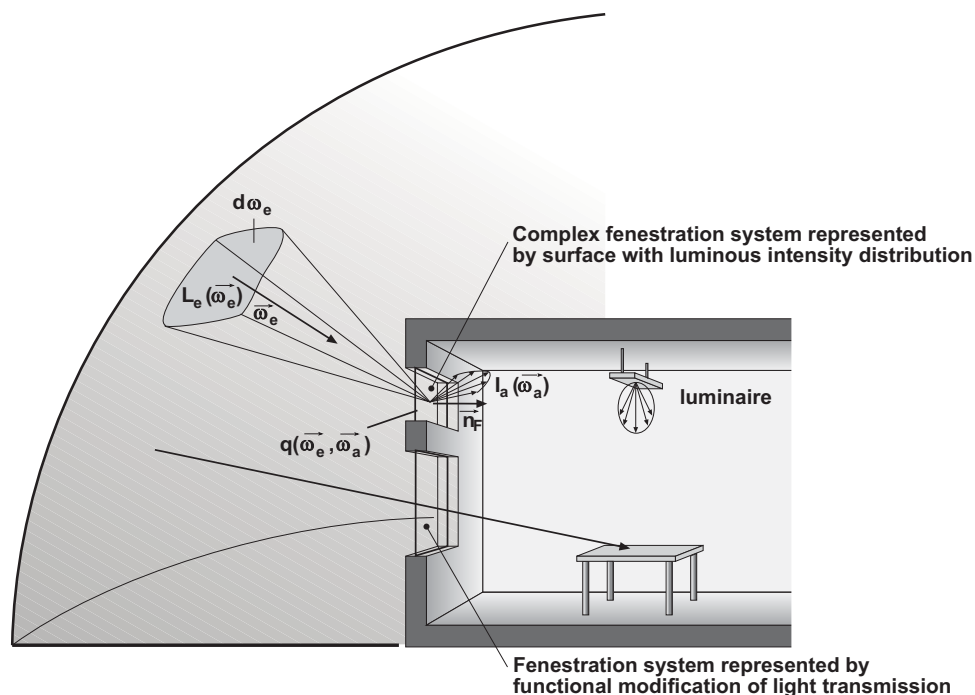


Figure 5: Schematic representation of the developed calculation method to determine room illumination through CFS. Instead of a conventional functional modification of daylight transmittance (e.g. by standard glazing), the external luminance distribution is converted into luminous intensity distributions, using the measured or computed façade system photometric parameters. These luminous intensity distributions are imprinted upon surfaces, which (by analogy with the calculative consideration of luminaires) illuminate the space.

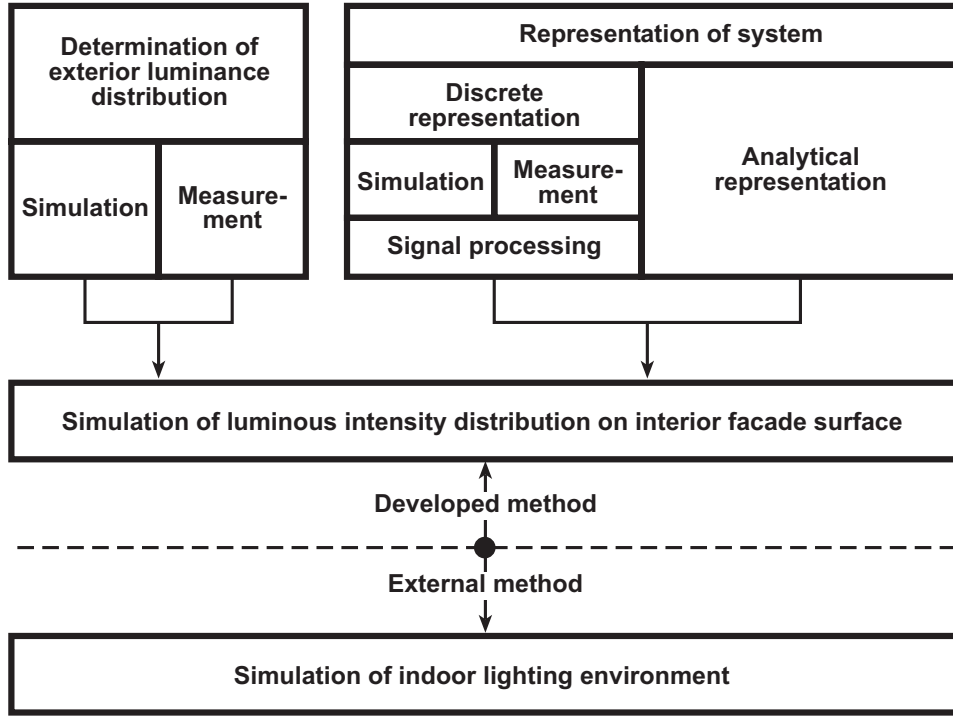


Figure 6: Scheme representing the calculative procedure for determining the room illumination by different CFS.

According to Figure 1, the internal luminance distribution $L_a(\vec{\omega})$ of the light-emerging surface will result from the incident-side external luminance distribution $L_e(\vec{\omega})$ and the luminous coefficient $q(\vec{\omega}_e, \vec{\omega}_a)$ (which describes the transmittance behaviour), from the internal luminance distribution $L_r(\vec{\omega})$ and the luminous coefficient $q(\vec{\omega}_r, \vec{\omega}_a)$ (which describes the internal reflection):

$$L_a(\vec{\omega}_a) = \int_{\Omega_{e,F}} L_e(\vec{\omega}_e) \cdot q(\vec{\omega}_e, \vec{\omega}_a) \cdot \langle -\vec{n}_F, \omega_e \rangle \cdot d\omega_e + \int_{\Omega_{r,F}} L_r(\vec{\omega}_r) \cdot q(\vec{\omega}_r, \vec{\omega}_a) \cdot \langle \vec{n}_F, \omega_r \rangle \cdot d\omega_r \quad [\text{cd}/\text{m}^2] \quad (4)$$

The first summand of equation (4) describes the luminance induced by transmittance through the façade element; the second summand describes the luminance due to the interior retro-reflection. The luminous intensity distribution $I_a(\vec{\omega})$ of the light-emerging surface can be determined immediately from $L_a(\vec{\omega})$ by way of

$$I_a(\vec{\omega}_a) = L_a(\vec{\omega}_a) \cdot A_F \cdot \langle \vec{n}_F, \vec{\omega}_a \rangle. \quad (5)$$

The incident-side luminance distribution $L_e(\vec{\omega})$ of the hemisphere over the façade element will be split up into diffuse lighting and direct sun light, as commonly done with sky models and within calculation programmes:

$$L_e(\vec{\omega}_e) = L_{e,diff}(\vec{\omega}_e) + L_{S,m} \cdot \text{rect}_{\Omega_S}(\vec{\omega}_e) \quad (6)$$

where

$$\text{rect}_{\Omega_S}(\omega) = \begin{cases} 1 & \text{for } \omega \in \Omega_S \\ 0 & \text{otherwise} \end{cases} \quad (7)$$

The sky component of the diffuse light incidence $L_{e,diff}(\vec{\omega})$ will mostly be described by way of continuous, (in sections) steady functions [21], [22]. The luminance distribution on premises and outside obstructions may be determined analytically or, in case of more complex geometries, also numerically [7], [8]. Normally, the external luminance distribution shows discontinuities at the transition between sky and terrain and at building-obstructions. Besides analytical descriptions, sky scanner recordings of discrete external luminance distributions [23] are also used – mainly for purposes of research. As the sun is a big discontinuity in the sky hemisphere, it will be considered separately. The internal luminance distribution $L_r(\vec{\omega})$ is not known a priori. It is a function of the light flux entering the room and of the space parameters. The light simulation programme must determine this value by iteration. The luminous coefficients $q(\vec{\omega}_e, \vec{\omega}_a)$ and $q(\vec{\omega}_r, \vec{\omega}_a)$ may be available either as functional values or as measured data. If the luminous coefficients and incident-side luminance distributions $L_e(\vec{\omega})$ and $L_r(\vec{\omega})$ are available as functional descriptions, the integral in equation (4) can be solved directly. In this case, however, the equation must be solved numerically as this approach is based on measured data.

The implementation of equation (4) in a calculation procedure follows the subdivision of the hemispherical luminance distribution over the façade unit acc. to equation (6) by determination and superposition of the diffuse and direct daylighting components in accordance with:

$$L_a(\vec{\omega}_a) = L_{a,diff}(\vec{\omega}_a) + L_{a,S}(\vec{\omega}_a). \quad (8)$$

The following subsections separately describe the determination of the component under diffuse illumination $L_{a,diff}(\vec{\omega}_a)$ and the determination of the component under direct illumination $L_{a,S}(\vec{\omega}_a)$.

3.1 Light transmittance under diffuse illumination

The indicatrices of diffusion for discrete angles of incidence $\vec{\omega}_{e,i}$ are determined by measurement, which generally represent the centre of various solid angles Ω_i of a hemispherical discretization. In practice, the Tregenza model [3] is used for hemispherical discretization. As the diffuse external luminance of a solid angle Ω_i either the point luminance $L_{e,diff}(\vec{\omega}_{e,i})$ may be assumed or the mean luminance, which better describes possible variations of the luminance in the solid angle element i :

$$L_{e,m,i} = \frac{1}{\Omega_i} \int_{\Omega_i} L_{e,diff}(\vec{\omega}_e) \cdot d\omega_e . \quad (9)$$

For the discretized external luminance distribution hence holds:

$$L_{e,d,diff}(\vec{\omega}_e) = \sum_{i=1}^N L_{e,m,i} \cdot \text{rect}_{\Omega_i}(\vec{\omega}_e) \quad (10)$$

where

$$\text{rect}_{\Omega_i}(\omega) = \begin{cases} 1 & \text{for } \omega \in \Omega_i \\ 0 & \text{otherwise} \end{cases}$$

with N indicating the number of solid angle elements. For the hemispherical discretization according to Tregenza $N=145$ holds.

In signal theory, averaging in equation (9) corresponds to low-pass filtering and thus to damping high-frequency components of the original external luminance distribution. The not exactly equidistant hemispherical discretization according to Tregenza is done in angular steps of about 12° , thus setting the filter width for averaging. In Figure 7, sections through several selected external luminance distributions are compared to their respective, filtered versions. Including the supplementary representation of

the Fourier transform's amplitude spectrum it becomes clear that the agreement of the original distribution and the filtered one is quite good, both for the overcast day and for the strongly varying CIE clear sky, for an assumed solar altitude of 20° (which in Figure 7 corresponds to an angle of 70° between zenith and sun). Taking a look at a large discontinuity in the external luminance distribution at a hypothetical external obstruction, the low-pass characteristic, which causes local damping of the discontinuity, becomes evident. The distribution's spatial resolution changes at the discontinuity, but not so the average of the total luminance distribution. These examples suggest that the common CIE sky models may be assumed to render a sufficiently good representation of luminance dynamics by discretization and filtering acc. to equations (9) and (10). Actual external luminance distributions, measured by means of sky scanners [23], are usually also read at 145 measuring points, according to Tregenza. Here, the measured data are also mean values averaged over the respective solid angles. The representation of $L_{e,d,diff}(\vec{\omega})$, based on measured data, thus directly satisfies equations (9) and (10).

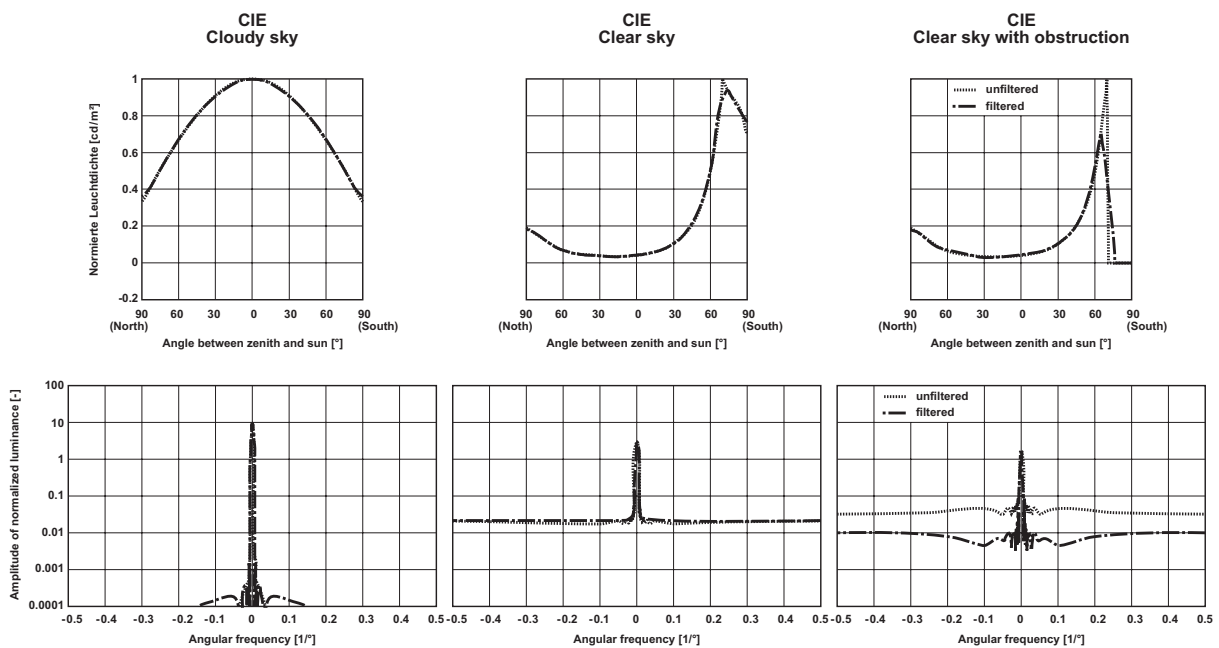


Figure 7: Sections through selected, normalized external luminance distributions (top) and associated amplitudes of the Fourier transform (bottom) over a horizontally oriented façade component. The sections through clear sky distributions are lying within the plane spanned by the sun, the zenith, and the point of origin.

Interpreting the external luminance distribution $L_{e,diff}(\vec{\omega})$ acc. to equation (10) as object domain in terms of Fourier optics [10], and understanding the associated, incident-angle dependent indicatrices of diffusion $q(\vec{\omega}_{e,i}, \vec{\omega}_a)$ as point spread functions (i.e. as impulse response functions of optical systems), the interior luminance distribution $L_{a,diff}(\vec{\omega})$ (the image domain in Fourier optics) will result as the sum of the convolutions

$$L_{a,diff}(\vec{\omega}_a) = \sum_{i=1}^N L_{e,m,i} \cdot \text{rect}_{\Omega_i}(\vec{\omega}_e) * q(\vec{\omega}_{e,i}, -\vec{\omega}_e) \cdot \Omega_i \langle -\vec{n}_F, \vec{\omega}_{e,i} \rangle. \quad (11)$$

As convolutions are performed with the approximately low-pass limited signal $\text{rect}_{\Omega_i}(\vec{\omega})$, the image function is also subject to low-pass limitation. High frequency characteristics of the indicatrices of diffusion are as well strongly damped. To determine the diffuse light transmittance through the CFS it is therefore sufficient to have approximate indicatrices of diffusion, the discretization of which corresponds to the incident-side hemispherical discretization. With regard to the numerical implementation, filter conditions can thus be derived for the indicatrices of diffusion, which are normally recorded with distinctly smaller angular distances, i.e. with higher resolutions.

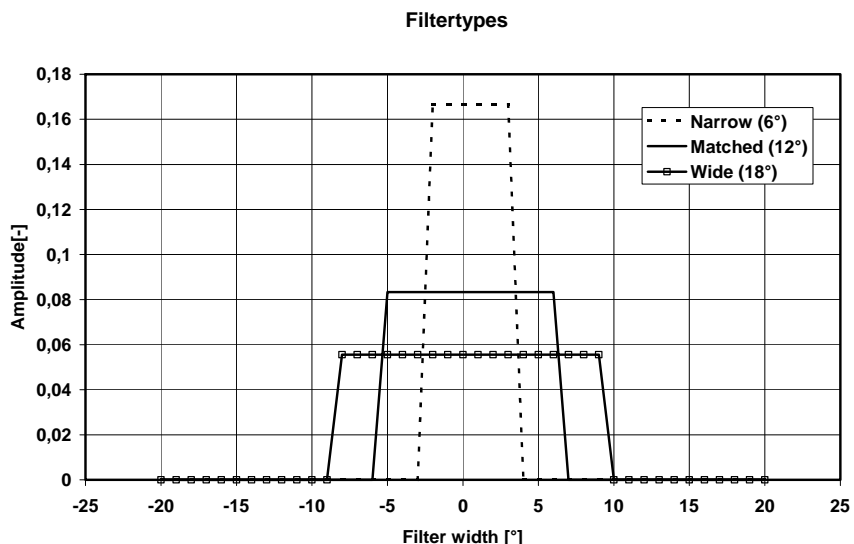
Equation (11) is transformed as follows:

$$L_{a,diff}(\vec{\omega}_a) = \sum_{i=1}^N L_{e,i,m} \cdot q_{fi}(\vec{\omega}_{e,i}, \vec{\omega}_a) \cdot \Omega_i \langle -\vec{n}_F, \vec{\omega}_{e,i} \rangle \quad (12)$$

with the filtered indicatrix of diffusion holding

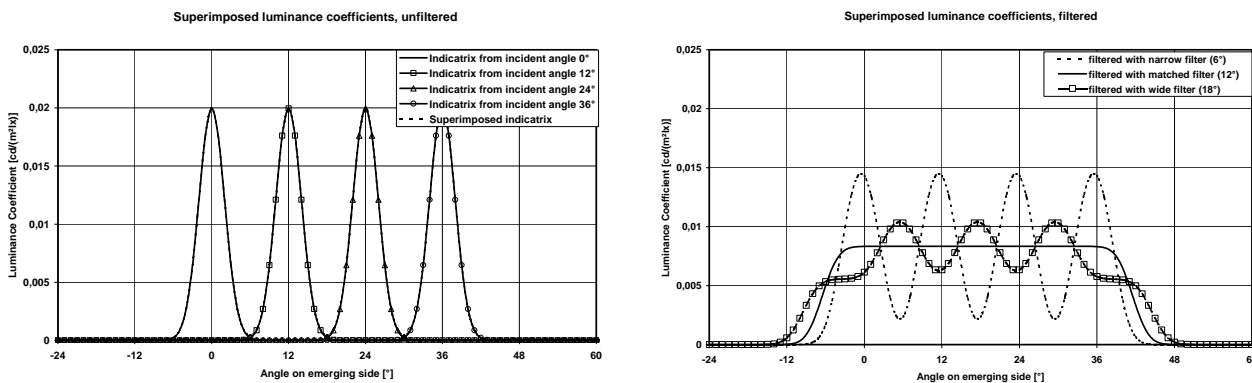
$$q_{fi}(\vec{\omega}_{e,i}, \vec{\omega}_a) = \text{rect}_{\Omega_i}(\vec{\omega}_e) * q(\vec{\omega}_{e,i}, -\vec{\omega}_e). \quad (13)$$

Figure 8 exemplarily illustrates the convolution operations for two types of systems and a variation of three filters. A sample with strong spatial resolved light transmittance (e.g. clear glazing) and a sample with a rather wide indicatrix of diffusion, i.e. little spatial resolution, are considered. The left hand side of Figure 8 b) illustrates the superposition of the unfiltered luminance coefficients as function of the altitude angle (emerging side), the figures on the right hand side show the filtered data for the three types of filters illustrated in Figure 8 a).

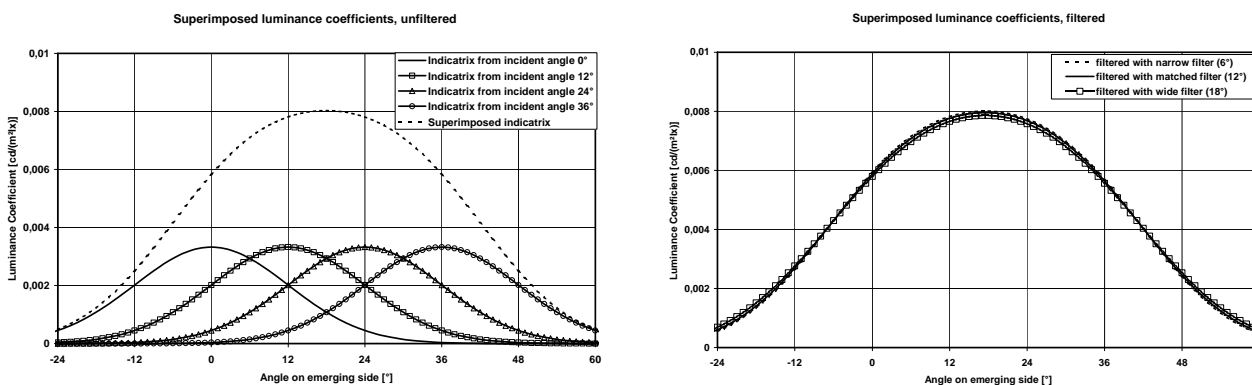


(a) Considered filter types

Big spatial resolution



Little spatial resolution




(b) Superimposed  icatrices: left figures unfiltered indicatrices; right figures filtered indicatrizes.

Figure 8: Different filter types (mean filters) applied to superimposed indicatrizes of diffusion, which show either a big or a little spatial resolution.

For a clear glazing, under uniform illumination the expected even distribution is only achieved for the matched filter, with the filter width, as derived from the sky hemisphere subdivision with an angular sampling distance of approximately 12° . For the narrow filter the peaks explicitly remain. For the wide filter artefacts, with peaks in between the raw data peaks become visible. For the scattered distribution, the sensitivity to the filter width is much lower, artefacts are lower.

Figure 9 presents a comparison between the superimposed original and filtered indicatrices of diffusion, for clear glazing in a top lighting situation under a CIE overcast sky. In the left-hand visualization, which presents the superposition of the original indicatrices of diffusion, the spatially high resolved "peaks" that were recorded for the 145 incident angles still remain. This causes an uneven "spotlight" type illumination when incorporated into a daylight simulation programme. In the right-hand visualization, the superposition of the filtered indicatrices of diffusion is displayed. Now the interior luminance distribution is smooth as to be expected. Minor fluctuations in the filtered luminance distribution are due to the fact that the hemispherical discretization into solid angle elements acc. to Tregenza is not exactly uniform and does not cover the entire hemisphere. As the filter conditions are derived from the incident-side solid angle elements according to equations (11) to (13), the incident-side discretization also affects the secondary-side convolution of data.

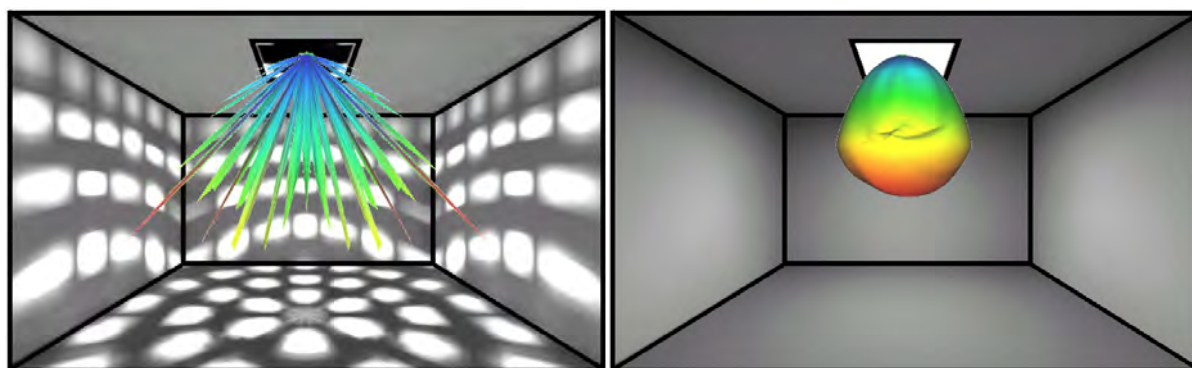


Figure 9: Illustration of the superposition of indicatrices of diffusion for a simple rooflight room situation with a clear glazing under a CIE overcast sky. Left-hand figure: Superposition of the *unfiltered* indicatrices of diffusion. Right-hand figure: Superimposed *filtered* indicatrices of diffusion.

In this way, the convolution according to equation (13) is a low-pass filtering of the indicatrix of diffusion. It is independent of the absolute value of the luminances $L_{e,m,i}$ of the respective solid angle and can therefore be calculated in advance. The signal energy of the filtered indicatrix as against that of the original indicatrix of diffusion is confined to a limited, smaller frequency domain. By sampling with larger angular distances, a more compact representation is achieved that is also more efficient in terms of data storage. As shown before, the angular sampling frequency according to the Tregenza method is about $1/12^\circ$. As the convolution in equation (13) is not done with an ideal low-pass limited filter, a sampling frequency of approximately $1/6^\circ$ was found to be suitable. This corresponds to a data set size of 529 values per incident angle.

3.2 Light transmittance under direct illumination

In case of direct insolation, the light flux incident on façades may amount to a multiple of the light flux resultant under diffuse skies. A great number of façade systems have therefore been specially adapted to respond to the substantial direct-light component prevalent under insolation. Hence, the determination of light transmittance under direct illumination is of big importance regarding the absolute amount and the transmittance direction. Unlike the quasi-continuous diffuse external luminance distribution, the sun has to be treated as a point source with regard to the usual resolution range of the measured data sets. The overall resolution under direct illumination is therefore being determined by the resolution of the indicatrices of diffusion. Therefore the existing, high-resolution structures in the indicatrices of diffusion will persist. This is why the resolution capability of the indicatrices of diffusion (which were determined by measurement or simulation in numerical goniophotometers) should not be reduced by signal processing. However, high resolution usually implies large volumes of raw data. These may amount to up to 15 megabytes for a static, axissymmetric system and be twice as much for non-symmetrical samples with 145 indicatrices of diffusion [1]. For automated systems a multiple of these data volumes has to be dealt with, as the different states of the system (e.g. varying slat inclines) must be considered in sufficiently precise discretization. From the user's point of view, the reduction of these data volumes is therefore desirable.

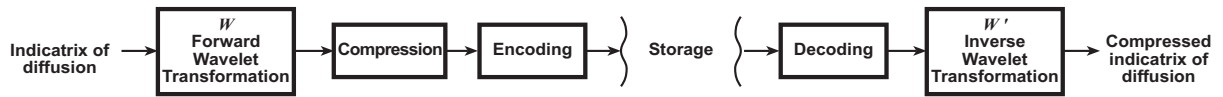


Figure 10: Data compression scheme: Data will first undergo a forward wavelet transform. Subsequently, the encoded transform coefficients will be stored. Signals are reconstructed by decoding the coefficients with a subsequent inverse wavelet transform.

Generally data compression methods are based on the decorrelation of raw data by way of integral transforms and subsequent filtering, mostly by setting the transform coefficient of low signal energy equal to zero. Setting coefficients to zero results in so called lossy compressions. The original signal can only be reconstructed with a certain accepted error margin with regard to the original signal. A schematic representation of signal processing is given in Figure 10. Here, the coefficients are obtained from mapping the raw data f onto a (generally orthonormalized) system of basis functions

$$c_i = \langle \psi_i, f \rangle. \quad (14)$$

The original data may then be presented as a linear combination of the set of basis functions:

$$f = \sum_i c[i] \cdot \psi_i. \quad (15)$$

The Fourier transform, which is widely used and important to many applications, represents the signal as a superposition of sinusoidal and cosine functions of different amplitudes and frequencies. Under aspects of data compression, the quality of a transform (and with this, also the selection of the basis functions) may be evaluated to the effect that the signal energy can be concentrated upon just a few transform coefficients. Tolerating minor deviations, the remaining coefficients can be set to zero, thus reducing the data volume to be dealt with. For distributions with strong resolution in the spatial domain (as is the case for indicatrices of diffusion of regular, direct transmitting materials, e.g. clear glazing, discussed in this context, or venetian blinds illuminated under certain incident angles), the Fourier transform is considered as inappropriate due to the periodicity of the basis functions. The same applies in spherical coordinate systems for transforms

based on spherical harmonics. For nearly complete signal reconstruction a comparatively large number of coefficients is needed, which cannot be set equal to zero. This is why achievable rates of compression are rather low. Using systems of wavelet basic functions [24], significantly more compact signal representations may be achieved for signals, which show a strong spatial resolution. For this reason, the measured indicatrix data are pre-processed (transformed and compressed) by way of a wavelet transform that was specifically adapted to spherical geometries [25].

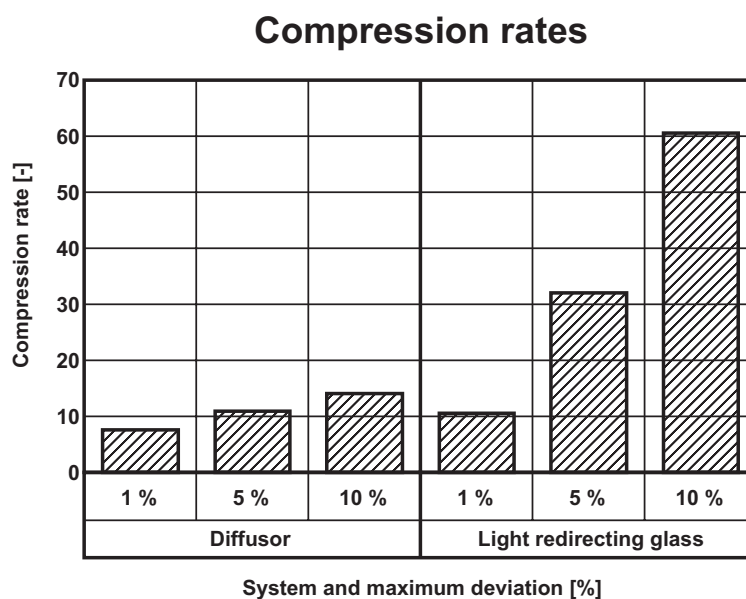


Figure 11: Comparison of mean compression rates for admitted deviations of 1%, 5% and 10% for a diffuse acrylic glass pane and a light redirecting glass [1].

In Figure 11 the achievable compression rates for the indicatrices of diffusion of a light redirecting glass and of a simple diffuser are given for various signal deviations. The rate of compression denotes the ratio between the original number of data points and the number of transform coefficients of the compressed signal. With a maximum deviation of 1 % between original signal and compressed signal, a mean compression rate > 10 can already be achieved for the light redirecting glazing. Here, a deviation of 1 % means that the smallest transform coefficients, altogether representing a signal energy of 1 %, are set equal to zero. For the diffuser's distribution, which is significantly less resolved, the rate of compression is about 7. The comparison suggests that higher rates of compression are achievable for the more resolved

distributions of the light redirecting glazing, compared to the diffuser. This shows that the wavelet transform's behaviour is inverse compared to the basis function system of Fourier transforms. A run-length coding device [24] is used for encoding the coefficients.

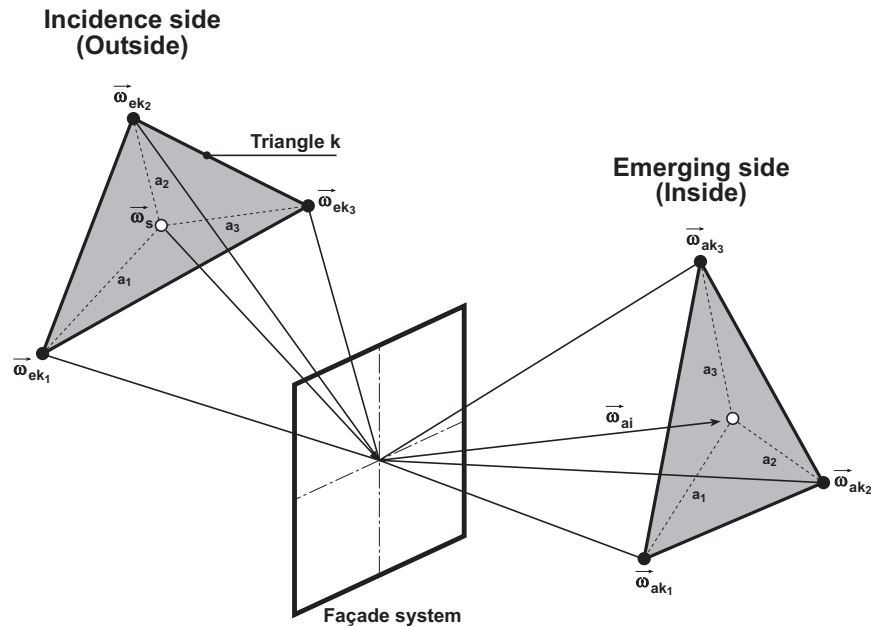


Figure 12: Mapping of continuous sun path: Geometrical relations of neighbouring incident angles, emerging-side characteristic vectors of indicatrices of diffusion for interpolating the indicatrices of diffusion under direct lighting. a_1 , a_2 , a_3 denote similarity measures.

As the indicatrices of diffusion are determined for discrete incident angles only, mapping the continuous path of the sun's orbit on these discrete angles will cause displacements regarding radiation within the image domain with spatially high resolved distributions. A method is required, which is able to determine the indicatrix of diffusion $q(\vec{\omega}_s, \vec{\omega}_a)$ for any solar position $\vec{\omega}_s$ from those indicatrices of diffusion that were measured for discrete incident angles only, preferably while maintaining the resolution. Interpolation procedures producing continuous transitions between two or more known distributions are well known in computer graphics as so-called morphing methods. They require identification of significant distribution characteristics, which are transferred from one distribution to the next one. In general, this identification has to be done manually for the distributions to be transferred. This may be achieved by tools [26] that are also performing the interpolation by applying the morphing method. Depending on the type of

distribution of neighbouring indicatrices of diffusion, this sophisticated scheme of interpolation can be approximated with simplified schemes in some cases:

- Mapping onto the next neighbour: This function presents the trivial case of the sun's position being mapped onto the next neighbour, using the associated indicatrix of diffusion. This type of mapping is sufficient in good approximation in the case of neighbouring indicatrices of diffusion, with little spatial resolution.

- Displacement of the next neighbour: Prior to displacing the immediately adjacent indicatrix of diffusion, a significant characteristic has to be identified, which is shared by all three distributions at neighbouring positions $\vec{\omega}_{a,k_1}, \vec{\omega}_{a,k_2}, \vec{\omega}_{a,k_3}$. According to Figure 12, the appropriately interpolated characteristic point $\vec{\omega}_{a,i}$ results from interpolation within the triangle spanned by vectors $\vec{\omega}_{a,k_1}, \vec{\omega}_{a,k_2}, \vec{\omega}_{a,k_3}$ by way of similarity measures a_1, a_2, a_3 . These measures are derived from the geometrical relations between $\vec{\omega}_s, \vec{\omega}_{e,k_1}, \vec{\omega}_{e,k_2}, \vec{\omega}_{e,k_3}$ on the incident side and can be understood as normalized inverse distances of the sun position to the closest neighbouring incident angles. The immediate neighbour's indicatrix of diffusion $q(\vec{\omega}_{e,k_j}, \vec{\omega}_a)$ is rotated into the determined point of displacement [27].

- Interpolation of the next neighbours: In the case of direct, angular-relation-maintaining light transmittance through for instance glazing, which is scattering diffusely around the direct transmitting direction (and also in the case of blinds in the direct transmittance range), interpolation can be done by way of displacement and weighted superposition of the neighbouring indicatrices of diffusion.

For the case of a system description that is based upon 145 incident directions, a triangulation with 258 triplet points results, which describes the particular neighbourhood relations. For any of these relations, the interpolation schemes can be individually determined. These may be quite different within one system, as for systems with slatted blinds, for instance. Automatic attribution of schemes seems desirable, but is not implemented in the present study. Assuming the sun to be a point source compared to the resolution of the indicatrix of diffusion, for the emerging-side luminance

distribution of the façade component under direct insolation as in equation (8) then holds:

$$L_{a,S}(\vec{\omega}_a) = L_{S,m} \cdot q(\vec{\omega}_S, \vec{\omega}_a) \cdot \Omega_S \cdot \langle \vec{n}_F, \vec{\omega}_S \rangle \quad (16)$$

4. Incorporation into daylight simulation

Regarding incorporation into daylight simulation programmes, photometric aspects as light reflections at the interior surface of the façade element and determination of room illumination in the façade nearfield have to be regarded. Variability of the façade condition (e.g. slat incline as function of the position of the sun) is to be considered. The functionality of the newly developed method will be supplied in form of an application programming interface (API) for integration into different lighting simulation engines. The method will be incorporated into selected programmes.

4.1 Photometric aspects

Inside reflection

Daylighting simulation programmes determine the component of light that is interreflected inside the room; the radiosity method uses iterative algorithms, whereas the ray-tracing technique employs recursive algorithms [6]. This is why $L_r(\vec{\omega}_r)$ as in equation (4) changes in the course of calculations. Hence, the second term in equation (4) cannot be determined in advance, but only during calculation of the illuminance conditions prevailing in the space. Ray-tracing techniques are capable of considering directional reflectance behaviour. Using radiosity methods [6], [7] it is however only possible to model surfaces with ideal diffuse reflection; therefore $q(\vec{\omega}_r, \vec{\omega}_a)$ has to be assumed to be constant for any pair of incidence and emerging side angles. This is why direction-dependent reflectance behaviour on an interior façade surface cannot generally be modelled with all lighting simulation programmes.

In normal, side-lit spaces the light flux that is reflected at the interior surface of a façade component is only a minor part of the total inter-reflected component. By analogy with the treatment of luminaires in artificial lighting simulation, retro-reflection may be neglected; also, it may be approximated by diffuse reflection ρ_{diff} (to be measured, if appropriate), if the simulation programme is capable of considering reflections at direct light sources. In

rooms like atria, for instance, which have a large transparent façade portion in relation to the total enclosing surface, the directional reflection at the interior façade surface may have an increased influence on the light distribution within, if the inside inter-reflection is high. In such cases, it may be reasonable to completely analyse the second term of equation (4). Actually, the algorithm could be enhanced here, but the enhancements for these special cases are considered beyond the scope of this study. Moreover, measurement-based system descriptions [1] so far do not contain any indicatrices of diffusion $q(\vec{\omega}_r, \vec{\omega}_a)$, which is partially due to limitations of measurement equipment, partially to an increased measuring effort. It is however desirable, that these indicatrices will be included in future studies.

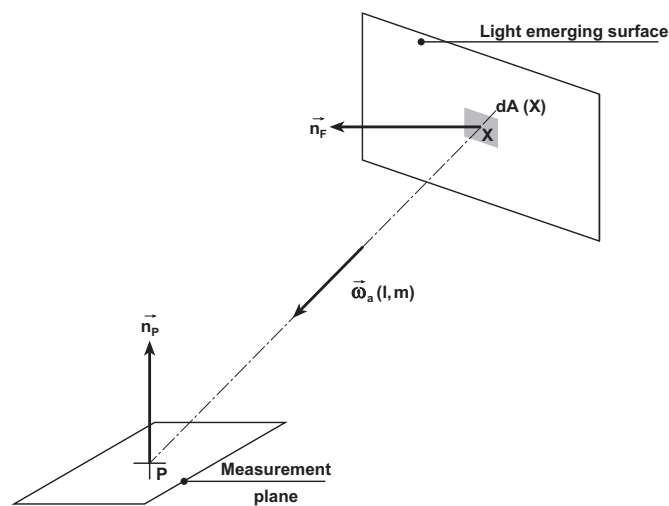


Figure 13: Geometrical relations of an internal point of observation P and the light-emerging surface.

Nearfield photometric aspects

The geometrical relation between the façade aperture and the enclosing surfaces (or points of measurement, respectively) rarely fulfils the farfield condition, under which the façade could be treated as a point source. As the case may be, the conditions required for working surfaces may be observed in high halls; in normal, side-lit rooms this is generally not the case. This is why nearfield conditions must be assumed for the interior. Figure 13 presents the direct illumination by some light-emerging, rectangular, plane surface with a homogeneous (i.e. constant across the surface) luminance distribution $L(\vec{\omega}_a)$. Determination of illuminance E at the point of observation P requires integration over the entire light-emerging surface:

$$E(P) = \int_{\chi} L(\vec{\omega}_a) \cdot \langle -\vec{\omega}_a, \vec{n}_P \rangle \cdot S(P, X) \frac{\langle \vec{\omega}_a, \vec{n}_F \rangle}{\|\vec{X} - \vec{P}\|^2} dA_F(X) \quad (17)$$

where $S(P, X)$ is a function describing visibility between points P and X . If there is a line of sight, this function is 1, otherwise it is 0. Here,

$$\vec{\omega}_a = \frac{\vec{X} - \vec{P}}{\|\vec{X} - \vec{P}\|} \quad (18)$$

represents the direction from point X towards point P . As $L(\vec{\omega}_a)$ is not functionally continuous but discrete, a direct solution for the correlation according to equation (17) (see Figure 13) cannot be given. The way in which the integration as in equation (17) is computed, depends on the light simulation programme applied. Proceeding on a finite element approach, the surface can be split up into subsurfaces with imprinted luminous intensity distributions, and the radiation from the subsurfaces can be superimposed in the point of measurement [8]. In [28] a rapid approach based on a Fourier series is developed, which applies only to restricted geometrical relations between the light-emerging surface and the surface that contains the point of measurement. For calculation tools that do not have an algorithm for integration acc. to equation (17), a method based on Monte Carlo Integration (originally developed for luminaires in [29]) is here transferred to the approach for determining the light transmittance through façades. In the so-called "Importance Sampling" of the Monte Carlo Integration, probability density distributions are given, which make it possible to achieve a small variance of illuminance $E(P)$ at a point P for a given, limited number of surface scanning points.

4.2 Dynamic systems

Dynamic façade components can be incorporated into control concepts for various control parameters. Positioning elements include stepping motors for moving blinds and modifying slat inclines, or switching units for controlling the light transmittance through electrochromic glazing. Control parameters may include façade-related direct illuminance, interior façade luminance distribution, time, switching patterns derived from user behaviour analyses, or

thermal quantities like indoor-air temperatures. Generally, these parameters are determined by the lighting simulation programme or from coupling with dynamic thermal computations, to be considered in façade modelling. In the present study, the following two control algorithms. Further functions may be provided.

- *Control algorithm according to DIN 5034:* German standard DIN 5034 [30] prescribes a simple way of controlling solar protection devices, which will activate solar shading devices once a façade is exposed to direct insolation. Modification of slat inclines of automated shading systems is not dealt with in this context.
- *Control algorithm based on characteristic system curves:* Numerous uniaxially controlled systems (like diverse slatted blinds, but also prismatic elements) only achieve maximum efficiency in narrow angular domains in relation to the position of the sun. Frequently, these systems are controlled by way of the façade-related solar profile angle. The solar profile angle represents the projection of the solar altitude angle onto a perpendicular plane, which is in a normal position to the plane of the façade. Depending on the system and the purpose of application, there are different requirements to the functional relation between the solar profile angle and the angle to be selected for the system. This relation is therefore described by characteristic curves, which are usually provided by the system manufacturers for integration into building control systems.

Figure 14 presents two exemplary, characteristic curves of daylight-redirecting blinds. Depending on the installation situation, the system may be operated either in a light-redirection mode (in the overhead area), or in a retro reflection mode (in the lower window area, which is critical with regard to glare problems). In addition, Figure 14 shows the so-called "cut-off" curve of a conventional blind system. The slats are adapted to the solar profile angle in such a way that any direct light incidence is prevented. The continuous characteristic curve must be mapped onto a sufficiently fine discretization of the slat inclines. According to manufacturers' specifications, a great many systems are operated in discrete increments of about 5°. A complete data set of indicatrices of diffusion then has to be provided for any slat angle position.

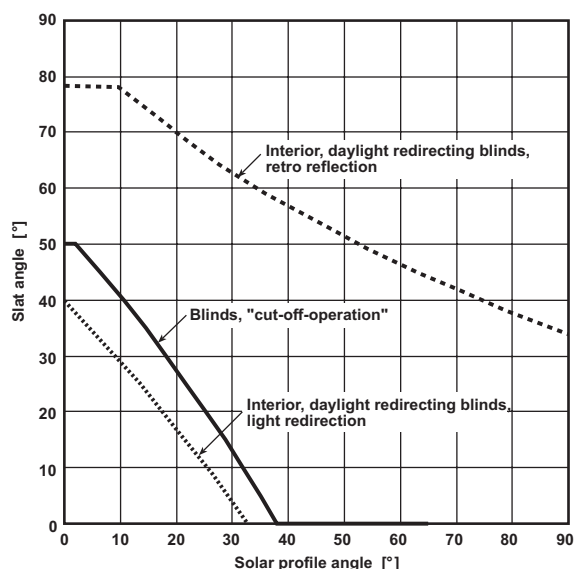


Figure 14: Characteristic curves describing the slat incline as function of the solar profile angle for conventional blind systems in the so-called "cut-off mode" and of a daylight-redirecting blind systems, which can be operated in two modes (retro-reflection and light redirection) [31].

4.3 Application Programming Interface

An Application Programming Interface (API) provides the central functionalities for computing the light-emerging surfaces. The API presented in this context comprises classes designed to

- specify the external luminance distributions,
- generate and read system description files,
- compute the luminous intensity distributions including parameterization of the calculation, and
- store the luminous intensity distributions in different luminaire data formats.

4.3 CFS database

The bidirectional light transmittance through CFS and the dependency on outside illuminance conditions deliver spatial and time variant indoor light penetration of generally much higher complexity compared to standard

glazing systems. These dependencies have to be made transparent to the designer in an easy to handle fashion, such that for specific problems the best solution can be identified at low expenses. Therefore a database with a graphical user-interface has been developed aiming at software support for CFS selection comparable to luminaire selection in artificial lighting programmes.

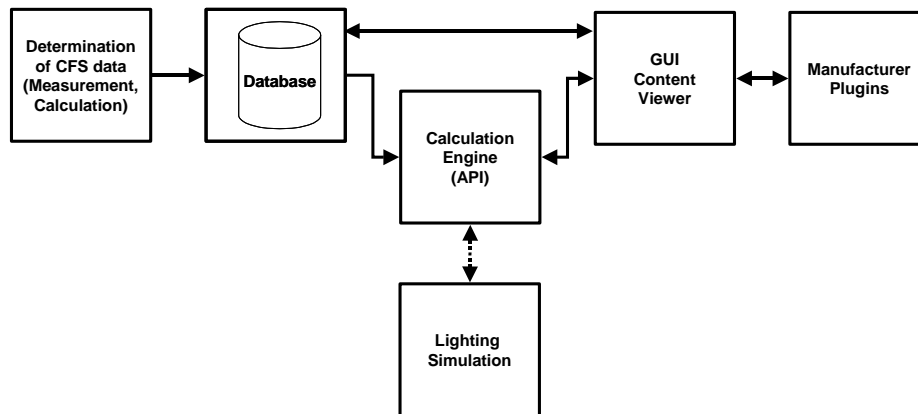


Figure 15: Structural diagram of data base system.

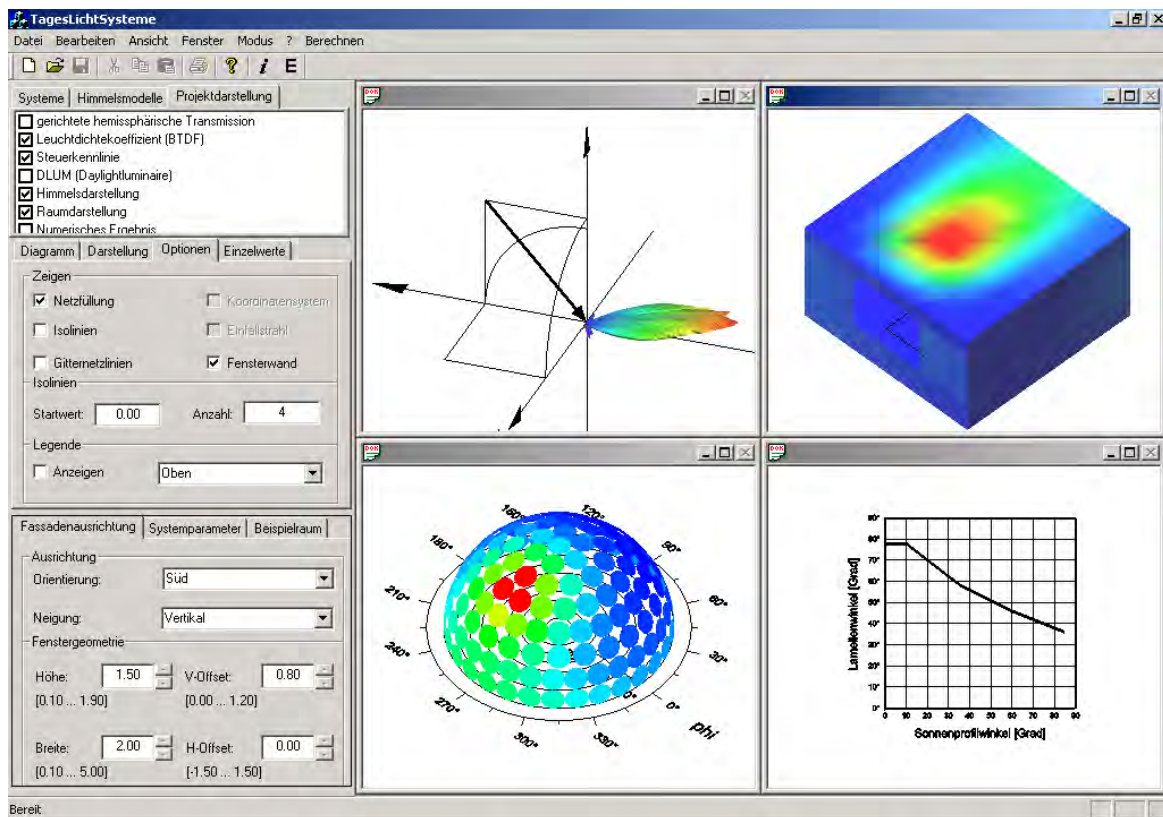


Figure 16: Screenshot of the database: Display of a BTDF, a sky luminance distribution, room illumination and control curve of blind system. Database will be available in English.

Within the CFS-database the API is used to illustrate room illumination caused by a selected CFS under definable outside luminance distribution.

4.4 Interfaces to lighting calculation engines

Programme modules based on the developed API have been integrated into RADIANCE and SUPERLITE, which are part of the ADELINe programme system [32]. To achieve this, the algorithms of both programmes were adapted to the effect that the external luminance distribution of the actually modelled scenario was computed and transferred to the novel programme modules, along with the CFS selected. The modules, which are called by RADIANCE or SUPERLITE, respectively, will then compute the luminous intensity distribution resulting for the respective CFS. The latter will be returned in formats proprietary to the programme. Both in RADIANCE and in SUPERLITE, the daylight transmitted through the specified CFS will be coupled into the space as part of the direct calculation. Figure 17 shows photorealistic visualizations and false colour representations of an office scene with different façade systems, generated by the modified version of RADIANCE. The represented façade systems include conventional blinds, light-redirecting blinds and light-redirecting glass. Using the other functionalities, that programme systems like [32] offer, it is also possible to investigate the impact of façade system on the lighting energy demand and internal loads over time. These results can then easily be linked into the thermal and energetical building performance analysis. Figure 18 shows the calculated electrical power demand for lighting purposes within a room for two different façade systems for south and west orientation on a sunny day. The calculation intervals can easily be extended to monthly or annual periods.

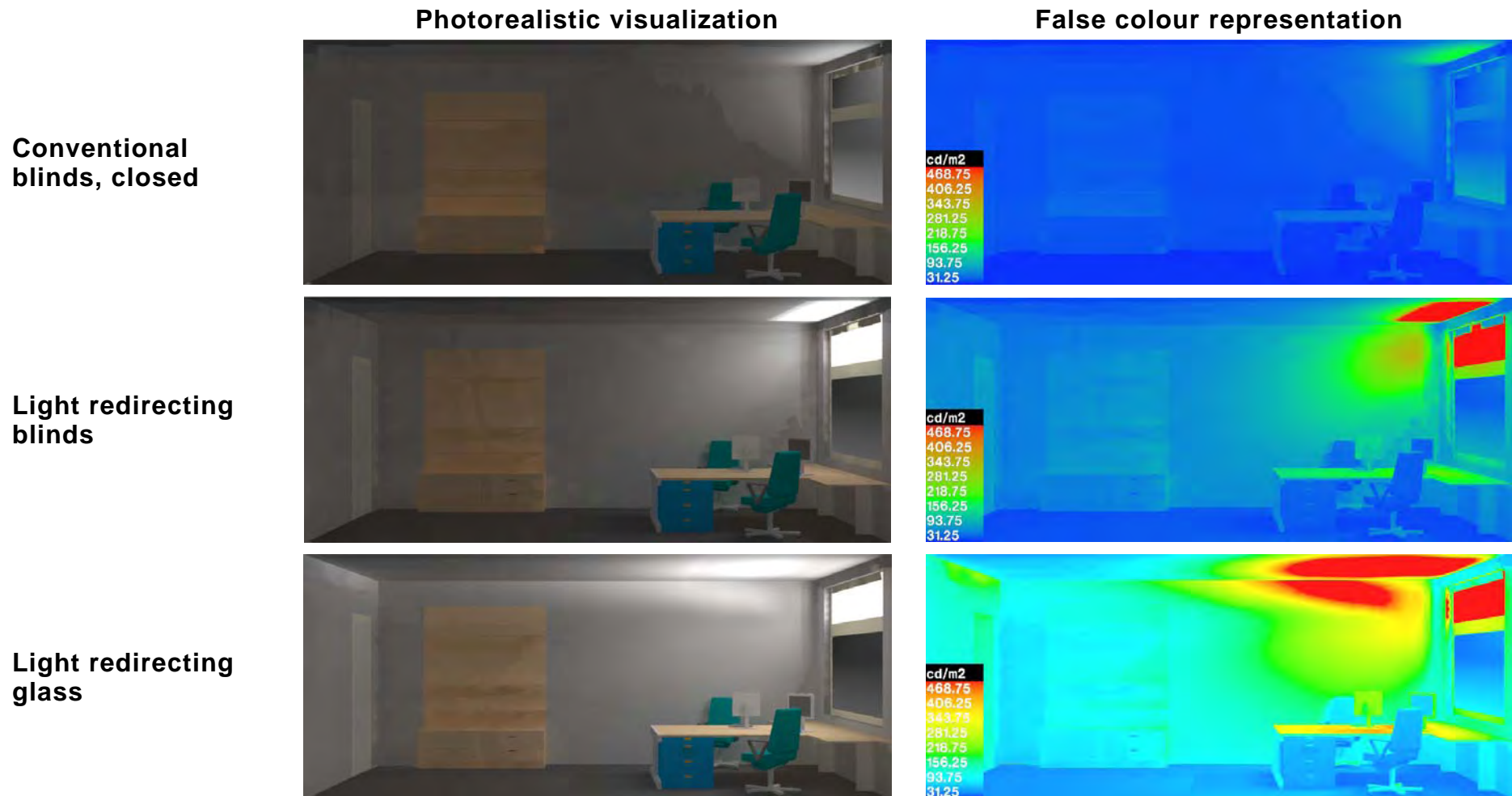


Figure 17: Photorealistic visualizations and false colour representations of the luminances in a south-oriented model space at noon on March 21 (equinox) for different façade systems. The visualizations were generated by RADIANCE, which was enhanced on the basis of the developed method for the computation of light transmittance through CFS.

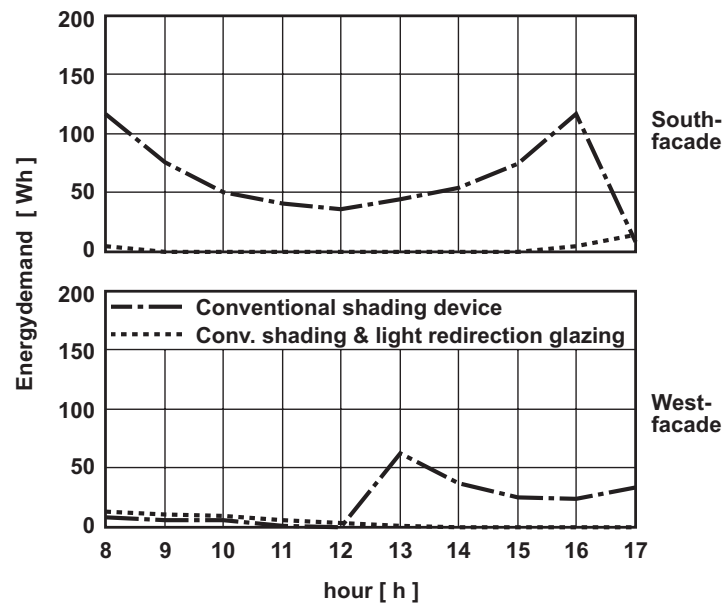


Figure 18: Comparison of the electrical power demand for lighting within a room for two different façade systems for south and west orientation on a sunny day.

5. Accuracy and validation

On the one hand, the accuracy of the newly developed calculation method is determined by the measured indicatrices of diffusion and the algorithm employed for processing external luminance distribution and indicatrices of diffusion to obtain the luminous intensity distributions. On the other hand, the daylight simulation programmes, which make use of the determined luminous intensity distributions, also have an influence on precision. In the following section, the effects of various procedural parameters regarding the accuracy of calculations and the limitations to the method will be dealt with. Subsequently, the procedure will be validated.

5.1 Accuracy

The following influences are relevant, namely:

Diffuse light transmittance

Under diffuse lighting, precision is given by the incident-side discretization of the hemisphere over the façade component (see 3.1). Concerning sky luminance distributions, which are relevant to daily design practice, sufficient accuracy may be assumed. Merely in case of major external luminance discontinuities, as may occur at obstructions, a tangible damping of light

transmittance through façade systems with indicatrices of diffusion with strong spatial resolution will result. If a higher level of accuracy is required, hemispherical discretization must be further refined. This implies a greater number of indicatrices of diffusion, or application of complex interpolation methods, which were mentioned before in the context of determining light transmittance under direct insolation.

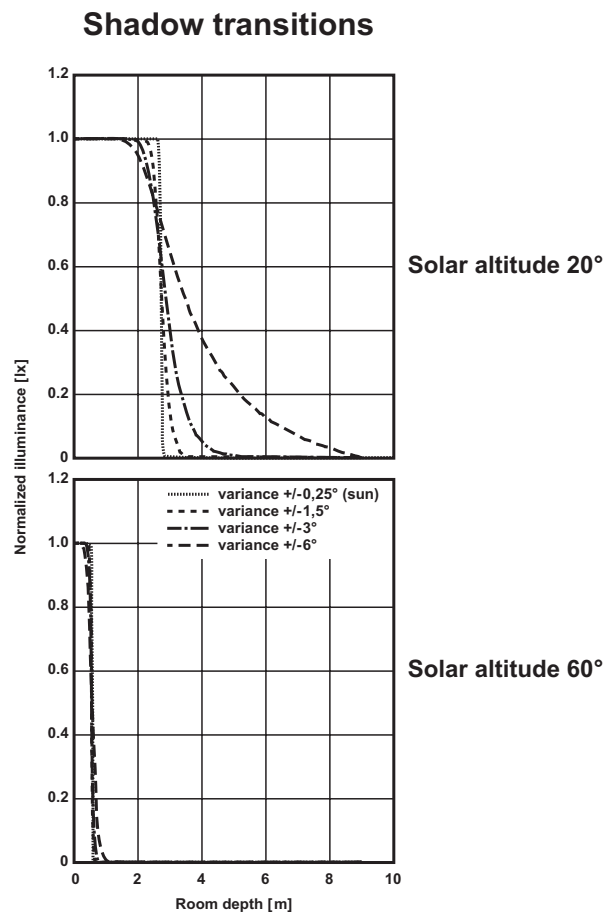


Figure 19: Shadow transitions of different local luminous intensity distributions on a horizontal plane, height of shadow border above room level: 1 m. In the upper diagram, the solar altitude is 20° , and 60° in the lower diagram. The variance of $\pm 0.25^\circ$ approximately corresponds to the opening angle of solar radiation.

Direct light transmittance

If the resolution of the goniophotometric measuring arrangement is smaller than the resolution of the indicatrix of diffusion of the real sample, the goniophotometric determination of the luminous coefficient enlarges sample variance. This will reduce the spatial resolution of the transmitted quasi-parallel sunrays compared to the real sample. As a consequence, the

sharpness of shadow transitions between façade system and adjoining enclosing surfaces will be reduced. Figure 19 presents shadow transitions of luminous intensity distributions for direct transmitting systems. The systems have been approximated by way of Gaussian distributions of different variances, for intersectional surfaces located at angular inclines of 20° and 60° in the sunlight path. A variance of $\pm 0.25^\circ$ is an approximation of the spread of real sunbeams. Particularly at low solar altitudes, the areas of out-of-focus shadow transitions will rapidly increase compared to the real opening angles of sunrays. This approximation of direct light transmittance is inherent to the method; it is predetermined by the resolution of the indicatrices of diffusion.

Farfield conditions outside

Farfield conditions must be respected when mapping the exterior environment onto the façade system. If this is not possible (in case of highly obstructed façades, for instance), the aperture has to be split up into subsurfaces, for all of which individual luminous intensity distributions will have to be computed.

Homogeneity of the luminous intensity distribution

For interior points of observation, the accuracy of direct illumination by the light-emerging surface depends on the homogeneity of the luminous intensity distribution across the façade system and on the way in which the algorithms integrate over the surfaces. A variety of façade systems have inhomogeneous luminous intensity distributions, like those occurring at the slats of venetian blinds. In the newly developed method, however, the façade components are approximated as homogeneously emitting surfaces that can be described by just one luminous intensity distribution. The approximation of these inhomogeneities by homogeneously emitting surfaces with respect to the illumination of interior measuring points must therefore be checked. For this purpose, the abstraction of periodical structural façade characteristics by way of periodically arranged spot-like point sources (see Figure 20) can be used. Up to a maximum spatial period of $h/10 = 0.1$ m of the arrangement of light sources, good accuracy may be obtained already at a minimum distance of 1 m towards the façade. Since the smallest structures (slats, for instance) of many systems range in this area or below, accuracy may even increase. With bigger spatial periods, deviations in the near-façade area will increase, such

that approximation by way of the newly developed method may produce inaccuracies; rather, precise results may only be accomplished at a greater distance from the façade. If accuracy criteria cannot be met for large-area façade structures like lightshelves, these are recommended to be 'classically' modelled as extended physical structures.

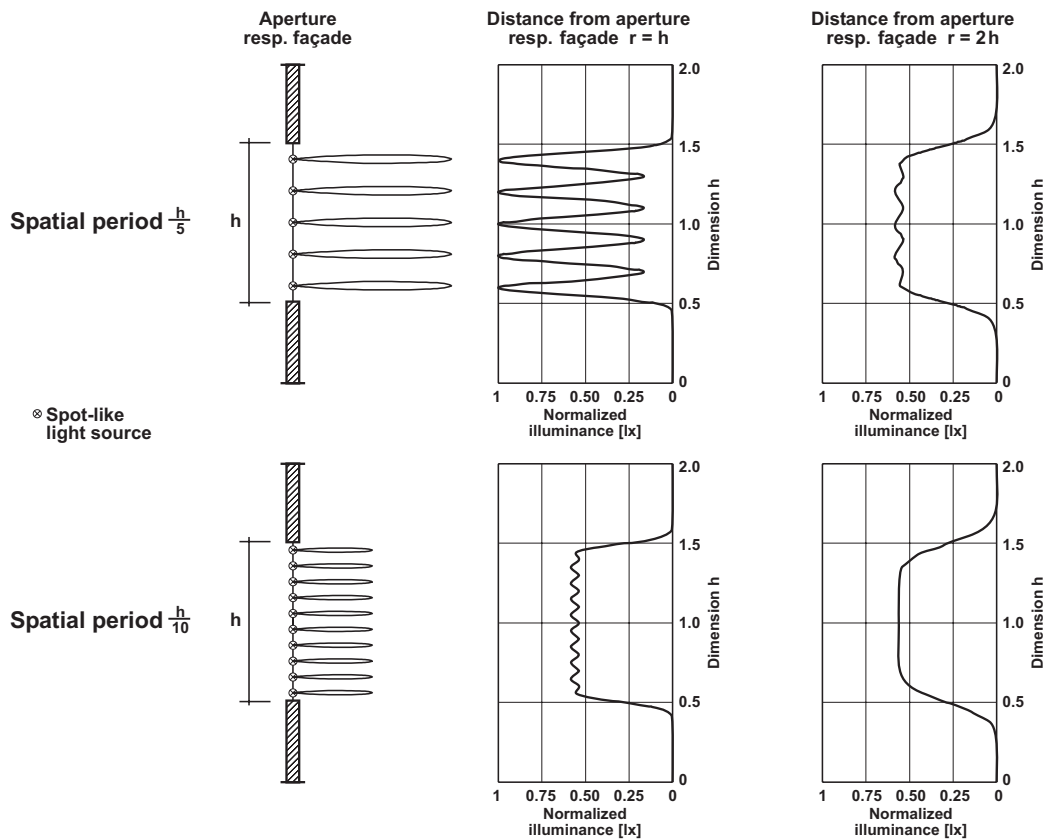


Figure 20: Illuminance distributions on sensor levels, as function of the distance towards a façade component with an inhomogeneous light distribution. The luminous intensity distribution on the façade is abstracted by periodically arranged spot sources. The upper diagram presents the interrelations for a spatial period of the light source arrangement of $h/5$, the lower diagram presents those for $h/10$. With an assumed height of the façade component of $h = 1$ m, spatial periods of 0.2 m (top) and 0.1 m (bottom) result.

Glare and resolution capability

Visual effects that may occur at edges or perforations of the rope guides of venetian blinds under very small solid angles, usually clearly exceed the resolution of the indicatrices of diffusion. The resolution capability of the human eye and, by this, the threshold of perception for this effect is

approximately one arc minute [33] for standard interior luminance adaptation levels, thus exceeding by far the resolution of indicatrices of diffusion that were determined by common-practice measurements. Such visual effects therefore cannot be evaluated by way of this method. Yet, this method is appropriate for giving general statements concerning visual comfort (such as meeting required mean façade luminance levels and interior luminance-dependent control of façade systems).

Visualizations

The macroscopic representation by way of indicatrices of diffusion does not contain any information about photometric properties of the actual material or about the system's geometry. Details of a façade system, like individual slats, for instance, cannot be represented in rendered images.

Dynamic façade systems

The modelling precision attainable for dynamic façade systems depends on the discretization of possible system states, like the slat inclines of venetian blinds or the switching mode of electrochromic glazing. To prevent direct light incidence in working areas, angular step widths for slatted blinds must be appropriately small. This requires a large number of system states to be measured or calculated. For instance, 21 complete indicatrix of diffusion data sets are needed for modelling a slat system that may be rotated by 100° at a required step width of 5° .

Determination of room illumination by lighting calculation programmes

The actual determination of the room lighting environment is done by external lighting simulation programmes, which use the determined luminous intensity distributions as internal sources of light. As set out earlier, the method developed in this study has been integrated in RADIANCE and SUPERLITE. Calculated luminous intensity distributions with big spatial resolutions require exact analysis of the integral in equation (17). The light-emerging surface must therefore be scanned with statistically sufficient accuracy. If the daylight calculation programme does not feature a suitable method, the approach implemented in the present paper may be applied.

5.2 Validation

The developed method is being validated by way of analytical reference cases and by results that were determined by means of calculation programmes validated earlier. Here, both the luminous intensity distributions of the light-emerging surfaces and the impact on room illumination are examined. The light transmittance due to diffuse and direct lighting will be examined in detail. Additional validation efforts for CFS with scale model measurements as reference can be found under [34], which also includes the new method presented in this paper.

The ideal diffuse and the ideal transparent façade system cover both limit states of light transmittance through façade systems. If these states are computed with sufficient accuracy according to the overall approach as in Figure 6, this can also be postulated for a great number of other systems, for the transmittance behaviour of which there are yet no closed analytical expressions and whose behaviour can only be described to a limited extent (if at all) by up-to-date calculation programmes. Examples for this type of systems are venetian blinds, the transmittance behaviour of which is a combination of highly diffusing and spatially highly resolved indicatrices of diffusion, depending on the respective slat angles. As a numerical model [11] exists for the laser cut panel, this more complex light-directing system will be examined in addition to the ideal diffuse and the ideal transparent façade systems. The following analytic reference distributions are obtained for a given, diffuse external luminance distribution $L_{e,diff}(\vec{\omega}_e)$. For the luminous intensity distribution of an ideal diffuser hence holds:

$$I_a(\vec{\omega}_a) = \langle n_F, \vec{\omega}_a \rangle \int_{\Omega_{e,F}} L_{e,diff}(\vec{\omega}_e) \cdot d\omega_e . \quad (19)$$

For the luminous intensity distribution of a transparent system applies:

$$I_a(\vec{\omega}_a) = \tau(\vec{\omega}_e) \cdot L_{e,diff}(\vec{\omega}_e) \cdot \langle n_F, \vec{\omega}_a \rangle . \quad (20)$$

For the external luminance distributions of overcast and clear skies [21], [22] analytically determined profile sections through the luminous intensity distributions of an ideal diffuser and an ideal transparent façade element (computed by way of equations (19) and (20)) are represented in Figure 21.

These are compared to the luminous intensity distributions that were calculated by the developed method. The transparent system was modelled as a system with ideal transmittance, assuming $\tau(\vec{\omega}_e) = 1$. Thus, it represents a façade aperture without glazing, i.e. with direct light transmittance. The method of numerical goniophotometry was applied to determine the indicatrices of diffusion required for establishing the radiation characteristics of the light-emerging surface. Agreement for the overcast sky is almost 100%. For the transparent system, the deviation of the calculated luminous intensity distribution under clear skies is due to the low-pass filtering effects of the convolution between the diffuse external luminance distribution (see equation (11) and the indicatrices of diffusion, which are determined for discrete incident directions only.

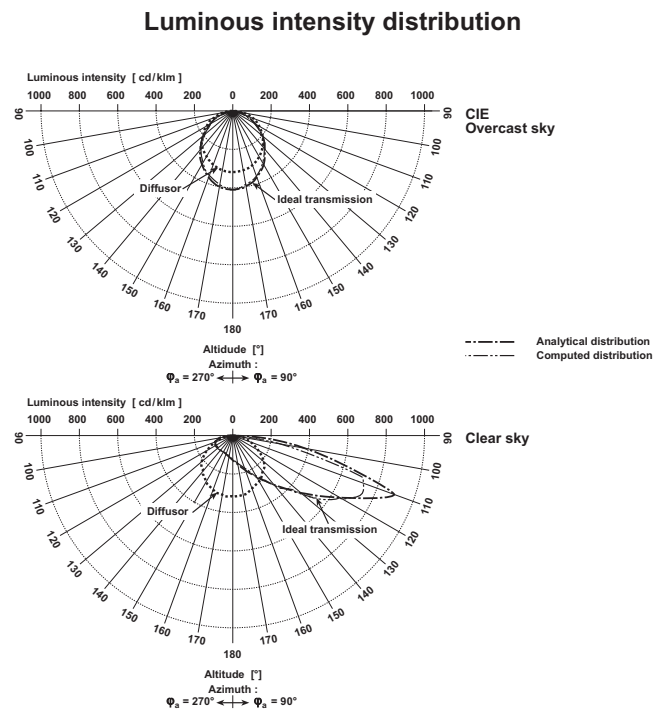


Figure 21: Comparison of sections through analytically determined luminous intensity distributions (normalized to 1000 lm) of an ideal diffuser and an ideal, transmitting façade system with those luminous intensity distributions determined by the developed method. The top diagram illustrates the distributions obtained by illumination with a CIE overcast sky. The bottom diagram presents the distributions caused by illumination with a CIE clear sky.

To determine the room's illumination level, the computed luminous intensity distributions were incorporated into the RADIANCE programme system. Figure 23 presents the illuminance sections determined for the horizontal and

vertical façade systems of the model spaces illustrated in Figure 22. To determine the relevant coupling of direct light into the room through the façade aperture, inter-reflections at the enclosing surfaces will be neglected for the present. The distributions generally show a good agreement. The RADIANCE model of the laser-cut panel, which was implemented according to [11] and serves as a reference case, shows a slightly increased overall light transmittance, thus implying higher illuminances. Deviations between the analytically determined (acc. to [11]) behaviour of the laser-cut panel and its numerically determined behaviour were already pointed out in [27]. In the analytical model, directional hemispherical light transmittances are higher. Figure 24 represents clear sky lighting conditions for a space with a vertical, ideal transparent façade, considering the inter-reflected component. A mean relative deviation of 5 % results.

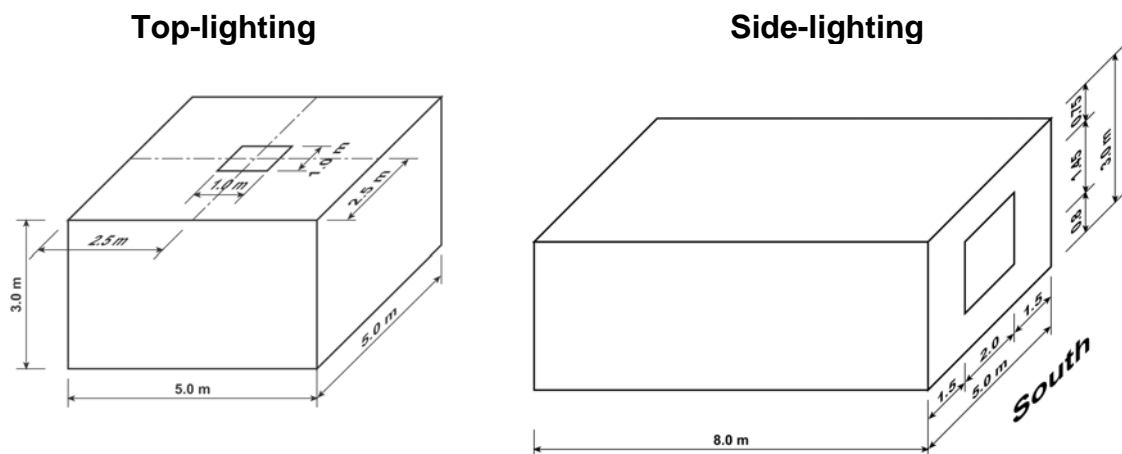


Figure 22: Isometries of the model spaces used for validating the developed calculation method.

According to equation (6), direct light transmittance has to be examined as a second component. For the inside (emerging side), maximum spatially resolved light transmittance through an ideally transparent façade, Figure 25 shows illuminance distributions at 0.1 m above the floor for the side-lit model space, at solar altitudes of 24° and 60° for different algorithms.

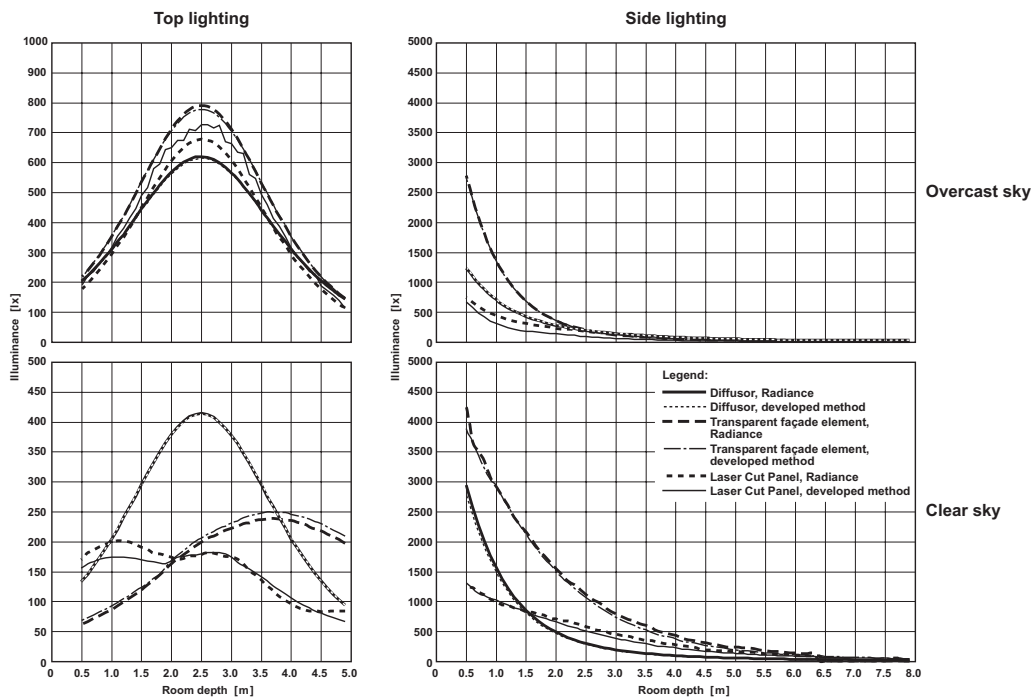
Direct component


Figure 23: Comparison of illuminance distributions on worksurfaces computed by the RADIANCE standard version [8] and by a modified RADIANCE version based on the developed method. The plots apply to top- and side lighting situations (see Figure 22) for the direct component (i.e. without inter-reflected component) at overcast and clear skies (solar altitude 20°) for three different types of façade systems.

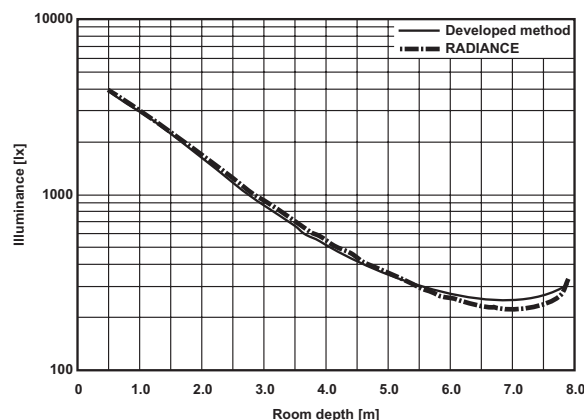
Direct- and interreflected components


Figure 24: Comparison of the illuminance distributions that were computed using the RADIANCE standard version [8] and by a modified RADIANCE version based on the developed method, as a function of room depth. Plots apply to a side lighting situation taking account of the interreflected component at a clear sky (solar altitude 20°) for an ideally transparent façade.

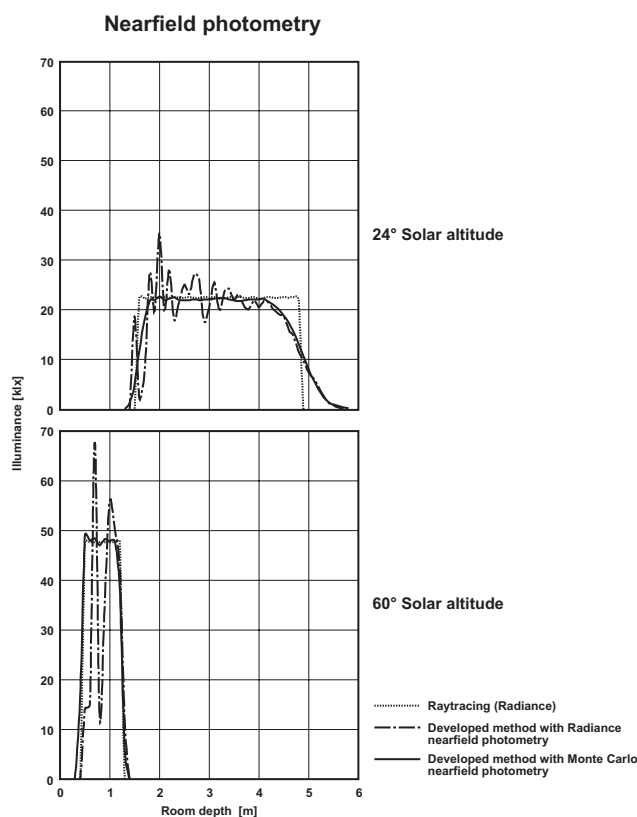


Figure 25: Comparison of the illuminances that were computed using the RADIANCE standard version [8] and by a modified RADIANCE version based on the developed method, as a function of room depth. Plots apply to a side lighting situation not considering the interreflected component, at direct insolation under 24° and 60°, without sky luminance distribution, for a façade with an ideal transmittance.

The ray-tracing algorithm that was chosen as the reference case precisely maps the direct light incidence following the laws of geometrical optics. If the lighting conditions are determined by way of the computed luminous intensity distribution, different curves will result, depending on the selected procedures of integration over the light-emerging surface according to equation (17). The RADIANCE standard algorithm for direct light calculations subdivides the light-emerging surface into a number of partial luminaires. The light emitted from these sub-luminaires is then superimposed at the point of observation. In addition, the scanning positions can be varied stochastically [8] over the sub-surfaces. The lighting conditions are represented correctly when averaged, but there are greater variances in the illuminance distribution at luminous intensity distributions, which have a high spatial resolution. Filtering over

several points of calculation may reduce these variances. To prevent glare problems, daylight designers generally try to avoid direct light incidence into working areas. Consequently, direct insolation is either totally excluded from the space, or it is allowed to enter working areas only indirectly, across the ceiling. In the majority of applications relevant to practical daylight planning, this implementation of equation (17) is applicable, as inter-reflections at mostly diffusely reflecting ceilings will increase the spread of the rays, thus considerably reducing variances. Direct calculation performed by way of the Monte Carlo Integration almost completely coincides with direct ray-tracing, which was chosen for reference purposes. This applies within the terms of the method-inherent, out-of-focus shadow transitions as previously discussed, which were shown to depend on the resolution of the indicatrices of diffusion.

6. Conclusion

Up to now, investigations concerning the influence of different CFS on natural illumination of indoor spaces were only valid under rigid boundary conditions. The quantification of the annual energy demand for supplementary (artificial) lighting as a function of complex façade design was merely possible. To overcome these limitations a new calculation method has been developed in the presented work, by means of which the effects of different façade designs on natural illumination of indoor spaces and the use of artificial light can be determined and evaluated. The calculation method is based on superimposing the external luminance distribution and the characteristic photometric parameters of the respective façade components, thus obtaining luminous intensity distributions. Façade components with both highly directional and diffuse transmittance properties (i.e. with indicatrices of diffusion, which can have low and/or high spatial resolution) are considered on the basis of measured data. Being imprinted upon virtual façade surfaces, luminous intensity distributions can be utilized in different lighting simulation programmes, by analogy with modelling artificial light sources.

To model light transmittance under diffuse illumination special filters for pre-processing the measured indicatrices of diffusion (BTDFs) were derived. Wavelet based data compression techniques are applied to the data allowing to significantly reduce the data volume of the indicatrices of diffusion.

Aspects of integrating the method into lighting simulation programmes are discussed, including nearfield photometric aspects and the consideration of dynamic (i.e. controlled, time-variant) façade elements. Based on a provided API (Application Programming Interface) the developed method has been integrated into two daylight simulation programmes and a CFS database. The accuracy of the method, which is significantly dominated by the recording procedure of the indicatrices of diffusion in goniophotometers, has been discussed. Validation has been performed against analytical and numerical test cases, indicating a generally good agreement. The calculation method is offered under www.talisys.de. The attached database as a platform for photometric data of CFS can be obtained for free under the same address.

7. References

- [1] Aydinli, H.; Kaase, H.: Measurement of Luminous Characteristics of Daylighting Materials. A Report of IEA SHCP TASK 21 / ECBSC ANNEX 29, Technical University of Berlin (1999).
- [2] Andersen, M.; de Boer, J.: Goniophotometry and assessment of bi-directional photometric properties of complex fenestration systems. Energy and Buildings, Under Review.
- [3] Tregenza, P.: Subdivision of the sky hemisphere for luminance measurements, Lighting Research and Technology 19, Nottingham (1987), H.1, pp. 13-14.
- [4] DIN EN 410: Glas im Bauwesen Bestimmung des Lichttransmissionsgrades, direkter Sonnenenergie-transmissionsgrad, Gesamtenergiedurchlassgrad, UV-Transmissionsgrad and damit zusammenhängende Glasdaten. Beuth Verlag, Berlin (1991).
- [5] WIS: Advanced Windows Information System, Calculation-Programme, Delft (1996).
- [6] Duin, H.; Symanzik, G.; Claussen, U.: Beleuchtungsalgorithmen in der Computergrafik. Springer-Verlag, Berlin, Heidelberg (1993).
- [7] Without editor: Superlite 1.0, Bedienhandbuch zum Lichtberechnungsprogramm. B.E.S.T. Gmbh, Stuttgart (1989).
- [8] Ward Larson, G.; Shakespeare, R.: Rendering with Radiance. Morgan Kaufmann, San Francisco (1998).

- [9] Autodesk: Lightscape 3.2: Concepts and Techniques in Computer-Generated Lighting Simulation. Autodesk White Paper, Autodesk Inc., San Rafael (2001).
- [10] Hecht, E.: Optik. 3. Auflage, Oldenbourg Verlag, München (2001).
- [11] Greenup, P. J.; Edmonds, I. R.; Compagnon, R.: Radiance algorithm to simulate laser-cut panel light-redirecting elements. Lighting Res. Technol. 32 (2000), H. 2, pp. 49-54.
- [12] Without editor: Lichtlenkglas Sgg Lumitop. Produktinformation der Firma Saint-Gobain Glass, Aachen (1999).
- [13] Jensen, H.: Global Illumination Using Photon Maps. In Rendering Techniques '96, Proceedings of the Seventh Eurographics Workshop on Rendering, New York (1996), pp. 21-30.
- [14] Raydirect, The Daylight Redirection Plug-In, Produktinformation unter www.schorsch.com (2003).
- [15] Mktis, Radiance Preprocessor to handle Daylight Redirection Systems, Internetseite der Fa. Exergia unter www.exergia.de (2003).
- [16] de Boer, J. : Numerical Goniophotometer. User Manual, Fraunhofer Institute for Building Physics, Stuttgart (2004).
- [17] Mitanchey, R.; Periole G.; Fontoynt, M.: Goniophotometric measurements: Numerical simulation for research and development applications. Lighting Res. and Technol., 27 (4), (1995), pp. 189-196.
- [18] Eggenstein, F.: Simulation von Tageslichtlenksystemen mit Radiance auf der Grundlage gemessener BTDF-Daten. Neuntes Symposium Innovative Lichttechnik in Gebäuden, Tagungsband, Otte Energie Kolleg, Kloster Banz (2003), pp.155-160.
- [19] Köster,H.: Entwicklung einer innovativen Tageslichttechnik, basierend auf optischen Spiegelsystemen, unter dem Gesichtspunkt der optischen and thermischen Behaglichkeit. Dissertation, Universität Karlsruhe (2002).
- [20] Dialux 3, Lighting calculation software. Dial GmbH, Luedenscheid, Internetsite under www.dial.de (2003).
- [21] CIE 110 -1994: Spatial Distribution of Daylight – Luminance Distributions of Various Reference Skies. Technical Report (1994).
- [22] CIE 22-1973: Standardisation of luminance distribution on clear skies. Wien (1973).
- [23] PRC-Krochmann, Sky Scanner, Photometer for Sky Luminance Distribution Measurement. Manufacturer Information PRC-Krochmann GmbH, Berlin (2004).

- [24] Bäni, W.: Wavelets, Eine Einführung für Ingenieure. Oldenbourg Verlag, München (2002).
- [25] Schroeder, P.; Sweldens, W.: Spherical Wavelets: Efficiently Representing Functions on the sphere. Computer Graphics Proceedings, Siggraph 95, ACM Siggraph (1995), pp.161-172.
- [26] Gourlay, M.: Xmorph, Image morphing program. Quellcode unter http://www.gnu.org/directory/All_GNU_PACKAGES/xmorph.html (2004).
- [27] de Boer, J.: Tageslichtbeleuchtung und Kunstlichteinsatz in Verwaltungsgebäuden mit unterschiedlichen Fassaden. PhD thesis, Universität Stuttgart (2004).
- [28] DiLaura, D.: On the computation of equivalent sphere illumination. Journal of IES (1975), Vol. 1, pp. 120 - 149.
- [29] Wang, C.: The direct lighting computation in global illumination methods. PHD thesis, University of Indiana (1994).
- [30] DIN 5034, Teil 3: Tageslicht in Innenräumen, Berechnung. Beuth Verlag, Berlin (1994).
- [31] Warema, Herstellerinformation zum Tageslichtlenksystem E80LD. (2001).
- [32] Dirksmöller, M.; Erhorn, H.: ADELIN 3.0. Documentation, Fraunhofer Institute for Building Physics, Stuttgart (1999).
- [33] Hentschel, H.-J.: Licht and Beleuchtung, Grundlagen and Anwendungen der Lichttechnik. 5. Auflage, Dr. Alfred Hüthig Verlag, Heidelberg (2002).
- [34] Maamari, F.; Andersen, M.; de Boer, J.; Carrol, W.; Greenup, P.: Experimental validation of simulation methods for bidirectional transmission properties. Energy and Buildings, Under Review.

8. List of Contact Persons

to be provided by OA Nancy Ruck

9. IEA Information

International Energy Agency

The International Energy Agency (IEA) was established in 1974 as an autonomous agency within the framework of the Economic Cooperation and Development (OECD) to carry out a comprehensive program of energy cooperation among its 25 member countries and the Commission of the European Communities.

An important part of the Agency's program involves collaboration in the research, development and demonstration of new energy technologies to reduce excessive reliance on imported oil, increase long-term energy security and reduce greenhouse gas emissions. The IEA's R&D activities are headed by the Committee on Energy Research and Technology (CERT) and supported by a small Secretariat staff, headquartered in Paris. In addition, three Working Parties are charged with monitoring the various collaborative energy agreements, identifying new areas for cooperation and advising the CERT on policy matters.

Collaborative programs in the various energy technology areas are conducted under Implementing Agreements, which are signed by contracting parties (government agencies or entities designated by them). There are currently 42 Implementing Agreements covering fossil fuel technologies, renewable energy technologies, efficient energy end-use technologies, nuclear fusion science and technology, and energy technology information centers.

IEA Solar Heating and Cooling Programme

The Solar Heating and Cooling Programme was one of the first IEA Implementing Agreements to be established. Since 1977, its 20 members have been collaborating to advance active solar, passive solar and photovoltaic technologies and their application in buildings.

Australia	Finland	Portugal
Austria	France	Spain
Belgium	Italy	Sweden
Canada	Mexico	Switzerland
Denmark	Netherlands	United Kingdom
European Commission	New Zealand	United States
Germany	Norway	

A total of 35 Tasks have been initiated, 25 of which have been completed. Each Task is managed by an Operating Agent from one of the participating countries. Overall control of the program rests with an Executive Committee comprised of one representative from each contracting party to the Implementing Agreement. In addition, a number of special ad hoc activities—working groups, conferences and workshops—have been organized.

The Tasks of the IEA Solar Heating and Cooling Programme, both completed and current, are as follows:

Completed Tasks:

- Task 1 *Investigation of the Performance of Solar Heating and Cooling Systems*
- Task 2 *Coordination of Solar Heating and Cooling R&D*
- Task 3 *Performance Testing of Solar Collectors*
- Task 4 *Development of an Insolation Handbook and Instrument Package*
- Task 5 *Use of Existing Meteorological Information for Solar Energy Application*
- Task 6 *Performance of Solar Systems Using Evacuated Collectors*
- Task 7 *Central Solar Heating Plants with Seasonal Storage*
- Task 8 *Passive and Hybrid Solar Low Energy Buildings*
- Task 9 *Solar Radiation and Pyranometry Studies*
- Task 10 *Solar Materials R&D*
- Task 11 *Passive and Hybrid Solar Commercial Buildings*
- Task 12 *Building Energy Analysis and Design Tools for Solar Applications*
- Task 13 *Advance Solar Low Energy Buildings*
- Task 14 *Advance Active Solar Energy Systems*

- Task 16 *Photovoltaics in Buildings*
- Task 17 *Measuring and Modeling Spectral Radiation*
- Task 18 *Advanced Glazing and Associated Materials for Solar and Building Applications*
- Task 19 *Solar Air Systems*
- Task 20 *Solar Energy in Building Renovation*
- Task 21 *Daylight in Buildings*
- Task 23 *Optimization of Solar Energy Use in Large Buildings*
- Task 22 *Building Energy Analysis Tools*
- Task 24 *Solar Procurement*
- Task 25 *Solar Assisted Air Conditioning of Buildings*
- Task 26 *Solar Combisystems*

Completed Working Groups:

- | | |
|--|-------------------------------------|
| <i>CSHPSS</i> | <i>ISOLDE</i> |
| <i>Materials in Solar Thermal Collectors</i> | <i>Evaluation of Task 13 Houses</i> |

Current Tasks:

- Task 27 *Performance of Solar Facade Components*
- Task 28/
ECBCS Annex 38 *Solar Sustainable Housing*
- Task 29 *Solar Crop Drying*
- Task 31 *Daylighting Buildings in the 21st Century*
- Task 32 *Advanced Storage Concepts for Solar Thermal Systems in Low Energy Buildings*
- Task 33 *Solar Heat for Industrial Processes*
- Task 34/
ECBCS Annex 43 *Testing and Validation of Building Energy Simulation Tools*
- Task 35 *PV/Thermal Systems*

Task Definition Phase:

Solar Resource Knowledge Management

To find more IEA Solar Heating and Cooling Programme publications or learn about the Programme visit our Internet site at www.iea-shc.org or contact the

SHC Executive Secretary, Pamela Murphy, e-mail:
pmurphy@MorseAssociatesInc.com.